MNE 23 (2024) 100261

Contents lists available at ScienceDirect

Micro and Nano Engineering

journal homepage: www.sciencedirect.com/journal/micro-and-nano-engineering

Review paper

Recent progress on gold nanoparticle biosensors monitored water quality: Insights on diversified contaminants and functionalization paradigms

Parth Malik [a,b], Ruma Rani [c], Rachna Gupta [d], Rakesh Kumar Ameta [e,*], Tapan Kumar Mukherjee [f,*]

[a] School of Chemical Sciences, Central University of Gujarat, Sector-30, 382030 Gandhinagar, India
[b] Swarrnim Startup and Innovation University, SSIU, Bhoyan Rathod, Gandhinagar 382420, Gujarat, India
[c] ICAR-National Research Centre on Equines, Hisar 125001, Haryana, India
[d] Department of Biotechnology, Visva-Bharati Santiniketan, Bolpur 731235, West-Bengal, India
[e] Department of Chemistry, Sri M M Patel Institute of Sciences & Research, Kadi Sarva Vishwavidhyalaya, Sector-15, 382015 Gandhinagar, Gujarat, India
[f] Amity Institute of Biotechnology, Amity University, Plot IIA-36, 37 &38, Action Area II, Rajarhat Newtown, Kolkata 700156, India

ARTICLE INFO

Keywords:
Water quality monitoring
Au nanoparticles based biosensors
Utmost sensitivity and reliable predictions
Functionalization
Limits of detection
Size and shape dependent physicochemical attributes

ABSTRACT

Over the past few years, water quality monitoring has swiftly emerged as a thrust area for most of the developing nations. Despite its renewable essence, incessant industrialization and urbanization have depleted the natural water resources, culminating in adverse impact on potable water quality. As a consequence, reliable technologies with utmost sensitivity and accurate predictions *vis-à-vis* authentic qualitative standards are urgently needed. Herein, interest in using gold nanoparticles (Au NPs) biosensors to gauge the qualitative profile of water resources has been quite significant. Major fascinations for Au NPs biosensing driven water quality monitoring are steadfast preparation methodologies, well-understood mechanisms for size-shape modulation and inert sensitivity manifested remarkable functionalization abilities. The size-shape modulated functionalization advances for Au NPs are the dynamic outcomes of their quantum effects, anchored *via* single or multidimensional quantum confinements (QCs). Morphologies as vibrant as rod, spherical, cylindrical, shells and combinatorial regime have been the backbone aspects of Au NPs based biosensors. With such insights, the present article focuses on last decade noted advances aimed at Au NPs biosensors assessed water quality. The studies discussed herewith were retrieved from Pubmed using the keywords, "Gold Nanoparticle Biosensors for Water Quality Monitoring". The knowledge shared herein could consolidate the fabrication of future Au nanomaterials based sensing technologies *vis-à-vis* functionalization mechanisms, cost considerations, precision aspects, integrated possibilities and long-term cautions.

1. Introduction

Deteriorating potable water quality has been an emerging global concern, manifested *via* unchecked human, industrial and agricultural exploitations. Pollutants from diversified sources (industrial and agricultural) contaminate the water bodies, rendering them unsafe for human consumption. Layman understanding of a contaminant *vis-à-vis* qualitative screening of any water resource implies any material prevailing at a more than optimum extent. Broadly, water contaminants can be chemical and biological, the former comprising insecticides, pesticides, aromatic compounds, heavy metals (HMs) *etc.*, the usual discards of industrial, agricultural and human activities. The mounting risk of all these contaminants relates to their persisting tendency with a non-biodegradable essence. Notable of these entities in the biological domain include humans, animals and microbial (fungal, bacterial and algal) excreta [1–3]. Emerging concern for declining water quality is well-inferred from the World Health Organization (WHO) recognition of "Safely Managed Drinking Water Services" as a global aim. Statistics report staggering 76 million annual cases of waterborne illness from United States [4]. Similarly, in Bangladesh, one of every five food poisoning deaths attributes to poor water quality [5]. Thereby, accurate, precise and reproducible detection of pollutants is the major step towards reclaiming freshwater resources for minimizing environmental and health damage [6,7]. Declining water quality on the global front is

* Corresponding authors.
E-mail addresses: ametarakesh40@gmail.com (R.K. Ameta), tapan400@gmail.com (T.K. Mukherjee).

https://doi.org/10.1016/j.mne.2024.100261
Received 10 November 2023; Received in revised form 10 May 2024; Accepted 14 May 2024
Available online 18 May 2024

aptly inferred by a mere 2.5% contribution of freshwater despite 70% of earth's surface being covered with water. More timid concerns include ~70% industrial wastes being dumped into water each year with 80% water pollution caused by domestic sewage. Estimates predict a staggering 6 billion pounds of garbage (majorly plastic) in oceans each year, with >4 lakh diarrhoea deaths due to polluted drinking water consumption. Shockingly, 368 million people use unsafe water globally with 80% land contributed wastes. The International Organization for Standardization (ISO) demarcates qualitative profile of water samples into I to III types, with type I being recognized as ultrapure (>18 MΩ-cm resistivity, $\sigma < 0.056$ μS•cm^{-1}, < 50 ppb total organic carbons).Corresponding nomenclature for drinking water are ISO24510 and ISO24511 while for wastewater is ISO24512. In India, decline in polluted rivers extent from 70% in 2015 (275 out of 390) to 46% in 2022 (279 out of 603) reflects awareness for conservation of water resources. However, increasing population, casualty for industrial effluent disposal has rendered 38.2% freshwater resources as polluted. As per 2018 Composite Water Management Index report, India ranks 120th amongst 122 countries on water quality index, with ~80.6% water being contaminated. Consensus for human consumption suited water deems (1–2) ppm as biological oxygen demand (BOD), (6.5–8) as optimum pH, (150–250) as total dissolved solids (TDS) as ideal. The physicochemical properties (PCPs) are more reliable than external energy driven UV spectroscopy, High Performance Liquid Chromatography (HPLC), Gas Chromatography (GC) [8,9]. A reliable aspect of PCPs is their temperature sensitivity as authentic qualitative indicators. For instance, recognition of *E. coli* strains (spreading fatal diseases) *via* incubation elapses 18–72 h to fetch reproducible results which could be done in (1–2) h using temperature specific density, ρ surface tension, γ and viscosity, η measurements [10].

Recent thrust into gold nanoparticles (Au NPs) with their high native stability and shape-size modulated quantum confinements (QCs) promises a well controlled, accurate and reproducible contaminants sensing *via* functionalized assays. A native inertness of Au (atomic number: 79, electronic configuration: [Xe] $4f^{14}$ $5d^{10}$ $6s^{1}$) entrusts Au NPs sensing advances *vis-a-vis* minimal cross-reaction risk with the corresponding analytes. Such attributes of Au NPs are the reasons for their portable, sensitive, automated and online feasible sensing configurations [11]. The efficacy of a biosensor is adjudged by probe-analyte specificity and sensitivity of transduction system intercepted analyte-probe biophysical interactions. Classification of biosensors could be made *via* screened analyte or workable detection mechanism. The detection mechanism based classifies configurations as electrochemical, calorimetric, optical and acoustic, characterized *via* differences in measurable prospects of probe-analyte combinations. A fair degree of similarity prevails in some types, such as electrochemical biosensors include both amperometric and potentiometric similar to optical fibre and surface plasmon resonance (SPR) regimen under optical regime. Incorporation of nanomaterials (NMs) simplifies the classification criteria, *via* specific NM based naming such as those using rod shaped NMs and quantum dots (QDs) being recognized as nanowire or QD based biosensors [12,13]. The rationale of amalgamating NMs in biosensors relates with their constricted energy levels driven prompt response, QC manifested alterations in optical, electronic and chemical properties. A prompt sensing of external stimulus in NMs is attributed to their high surface area (SA) manifested low E_a, whereby quick response to native energy levels is accomplished. The miniaturized dimensions of NMs make the sensing assembly robust and easy to relocate. A prominent distinction of NMs comprising sensors accounts for multifunctional probe sensitivity including temperature, pressure, optical, physical modulations due to missing quantum effects in bulk state. Analogy of this comparison could be understood *via* shrinking size of our electronic integrated circuits, whereby functionality is enhanced. Explicit benefit (s) for Au NPs relates to their distantly located 6 s sub-shell valence electron, which they can easily lose to form Au^{+} and readily couple with anionic surface sensitivity. Besides, the diversity of morphologies (rod, spherical, stars, shells and others) makes Au NPs suitable for a wide range of physical phenomenon and interacting receptiveness [13–16].

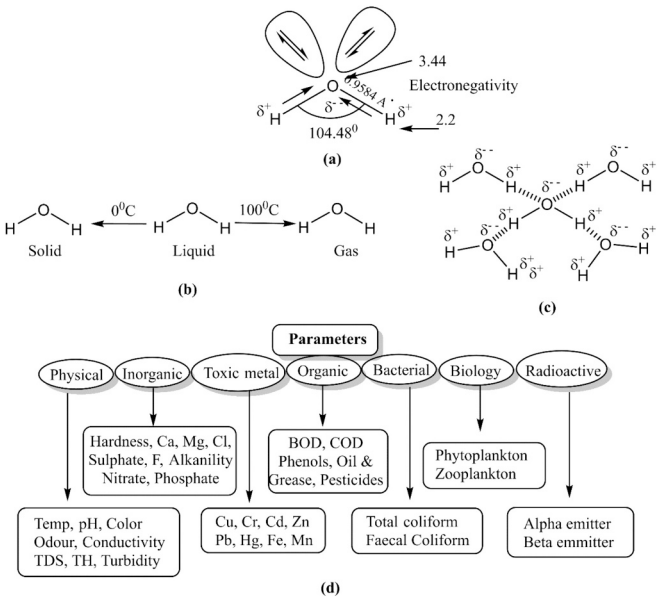

Fig. 1. Defining prospects of water, comprising its (a) Molecular structure with characteristic bond length and bond angle, (b) Temperature dependent prevalence of water in solid, liquid and gaseous states, (c) Possible inter and intra molecular hydrogen bonding attributing to a cage like networking of water molecules, (d) Native physical, chemical and biological attributes of water. With a polar nature and manifold usage, water has a unique ability of dissolving every substance to some extent, accounting for diversified contamination risks.

This article focuses on recent advances on Au NPs-biosensors monitored water quality. A high ground state stability conferred robust functionalization of Au NPs is the basis of not merely the sensing applications but also the targeted drug delivery where binding with specific cell surface receptors is needed. Readers are suggested to acquaint themselves with such distinctive abilities of Au NPs from the specific literature sources [17–19]. The unique optical traits of Au NPs, inspired by integrated oscillations of surface electrons are responsible for surface plasmon resonance (SPR). Surface plasmons (SPs) refer to the coherent electronic oscillations generated *via* electromagnetic radiations (EMR) at the metal-dielectric interface. Prominent optical sensitivities of Au NPs are explicit functions of dielectric environment and the EMR incident frequency. Herein, the SPR implication is manifested by resonance of oscillating SPs with incident EMRs, generating a characteristic stimulus at metal-dielectric interface [20,21]. The exclusive SPR frequency is decided by physical dimensions, morphology and chemical composition of NPs. For spherical regime, the resonant frequency falls within visible region of electromagnetic spectrum [22]. The high aspect ratio of Au NPs is sensitively affected by the dielectric nature of interacting vicinity (interfacial refractive index, RI) [23]. These features comprise physicochemical intricacies for analytes *via* interacting regimes substantiated surface absorption/desorption, aggregation and optical sensitivity. Analyte-detection corresponds to a binding extent proportionate SPR change of Au NPs, perceived *via* colorimetric changes [24,25]. Sensing platforms using Au NPs are optimized *via* enhanced localized electromagnetic field driven SPR changes. Such enhancements (Surface-Enhanced Raman Scattering) considerably improve the sensing sensitivity, distinctly identifying each target [26]. The robust functionalization techniques *vis-à-vis* NPs assembly on surface engineered platforms such as graphene and its derivatives encompass significant precision in electrochemical responses [27,28]. The shape-size controlled PCPs of Au NPs enable a precise detection of micro/nano-scale pollutants at parts per billion resolutions. Keeping above aspects in mind, hereby the major focus is on prospective attributes of Au NPs monitored water quality.

Table 1
Pure water standardized parameters as per WHO standards [34].

Parameter	Optimized range
pH	6.5–8.5
Turbidity (NTU)	1
Total Dissolved Solids (mg•L^{-1})	(150–250) but accepted till 500
Total hardness (as $CaCO_3$, mg•L^{-1})	200
Total alkalinity (as $CaCO_3$, mg•L^{-1})	200
Electrical conductance (μS•cm^{-1})	400

NTU: Nephelometric Turbidity Units.

Table 2
Native concentrations (mg•L^{-1}) of various ions fixed for water quality as per WHO standards [35,36]. The relative extents could ascertain the contamination extent.

Metal Ion	Ideal extents for potable water (μg•L^{-1})
Na^+	200
Ca^{2+}	100
Mg^{2+}	50
K^+	20
HCO_3^-	125–350
Cl^-	250
SO_4^{2-}	250
NO_3^-	50
Fe^{2+}	0.3
Mn^{2+}	0.1–0.5
Zn^{2+}	0.01–3
Al^{3+}	0.2
Pb^{2+}	0.01
Cu^{2+}	2
Cd^{2+}	0.003
Hg^{2+}	6 (For inorganic Hg)
Cr^{2+}	< 2
As	10
Se	40
U	30
F^-	1500

Emphasis has been paid to limit of detection (LOD) precision, selectivity, structural extensions and shape-size modulated PCPs.

2. Defining aspects of pure water and diversifications of contaminants

In its unadulterated form, water prevails as odourless, tasteless and colourless liquid with a bond angle of 104.48°, 0.9584 Å O—H bond length and an electronegativity of 3.44. Physical state of water varies with temperature, enabling a molecular distinction *via* varied intermolecular forces (Fig. 1). The intrinsic blueness of water is due to red light absorption [29]. With an ability to dissolve almost every material to a certain extent, water exhibits a highest density (1000 kg•m^{-3}) at 4 °C, prevailing in liquid state even at higher temperatures. In solid state (ice), the assembly of water molecules has one molecule as bonded to four others *via* intermolecular hydrogen bonding (HB), conferring strong cohesiveness, room temperature (RT) γ of 71.97 dynes•cm^{-1} and η as 0.8903 cP (Fig. 1b) [30–33]. Qualitative considerations on a global front distinguish the water resources as potable, palatable, contaminated and infected with surface water, oxygen depletion, nutrient, microbiological, groundwater and chemical mediated pollutions being distinguished. Screening of water quality is accomplished through physical, chemical and biological assessments Table 1 comprises the WHO recommendations for human usage compatible water traits, with acceptable TDS extents till 500. Human feasibility of water body could be adjudged by its high oxidation reduction potential (ORP), whereby plentiful oxygen implying a native cleansing ability *via* breakdown of waste products (contaminants, dead plants and animals) [34]. Table 2 comprises the regulatory guidelines recommended titre of ions in potable water, providing the basis for screening contamination [35,36]. Qualitative analysis could be accomplished *via* physical, chemical and biological assessments amongst which the physical standards (electrical conductivity, salinity, TDS, turbidity, melting and boiling points, odour, colour and taste) exhibit a highest consensus (Fig. 1d) [37,38].

Impurities in water are broadly distinguished on the basis of their biological or chemical origin, wherein the former includes the invasive and non-indigenous microbial species dwelling in a water sample. The biological and chemical contaminants affecting water quality are distinguished *via* microbial pathogens, excessive pesticides use, unmanaged industrial effluents, heavy metal prevalence (Fig. 2) [39–50]. Inceptive conceptualization of 'biological pollutants" was proposed by Elliott in 1972, considering them for invasion biology, *vis-à-vis* bacterial, algal and related toxins [51]. Though microbial contamination *via* improper wastewater management remains a biological concern, it can be tackled *via* pre-treating the toxic waste streams. Readers are advised to consult specific literature to have a better knowledge on microbial contaminant's health issues and environmental impacts [52–58]. Of late, microbial enzymes facilitated metallic NPs are being increasingly employed as remediation agents as several xenobiotics are easily degraded into simpler forms by microbes [59,60]. So, using recombinant DNA technology, the gene expressions controlling these enzymatic activities could be enhanced. Similarly, adversities of fertilizers and pesticides could be mitigated *via* nanocarrier mediated delivery [61–63]. Nanocarriers encompass a structural protection of delivered fertilizers and moderate the loading extents to counter undesired soil stress. Co-delivery of fertilizers with ecofriendly antioxidants safeguards them from oxidative damage, synergizing their antimicrobial activities with moderated administered quantities. Nonionic surfactants and plant extract capped NPs could be compatible stabilizers for such formulations, reducing the non-specific interactions [64].

3. Preparation methods for gold nanoparticles

With an atomic number of 79, Au exhibits [Xe] $4f^{14}$ $5d^{10}$ $6s^1$ electronic configuration. Owing to completely occupied energy shells, Au has a high ground state stability, minimizing the interfering possibility in sensing applications [65,66]. Preparation method for Au NPs (perhaps any singular metal NPs) comprises the reduction of chosen precursor salt, wherein zerovalent Au state (or the desired metal) is attained. The reduction of precursor salts could be accomplished *via* external energy (physical method), using microbial enzymes or plant metabolites (mostly natural polyphenols) or synthetic reducing agents (chemical method). The physical methods employ external energy, usually generate a lot of wastes and are environmentally threatening are the typical Top-down methodologies whereby no control in particle size dimensions could be exercised. Multiple methods using external energy as a source to reduce the metal salt precursors are known, such as laser beam ablation, ionic bombardment and others. Although the concerns of high energy dependence and enormous waste generation are resolved in chemical and biological methods for NPs preparation, the biological methods (nature friendly approaches using microbial enzymes or extracts of varied plant resources) suffer from scale up compatibility as the plant growth varies from one to other region [67–75]. Chemical methods of preparing metal NPs utilize the synthetic reducing agents and function without drastic energy inputs, enabling remarkable control in optimizing the particle dimensions *via* their "Bottom-Up" working principles (Fig. 3) [76–88]. Chemical methods of NPs preparation use moderate energy sources such as microwave treatment, emulsification, sustained ultrasonication (at low frequency), or a combination of these. The primed approach for Au NPs preparation was proposed by Turkevich, *via* varying precursor (mostly chloroauric acid, $HAuCl_4$)-reducing agent (trisodium citrate, $Na_3C_6H_5O_7$, sodium borohydride, $NaBH_4$ etc) interacting stoichiometries.

The nanoscale attributes of prepared NPs are explicit functions of their size-shape modulations, wherein a smaller size corresponds to stronger QC mediated changes in optical, physical, chemical and

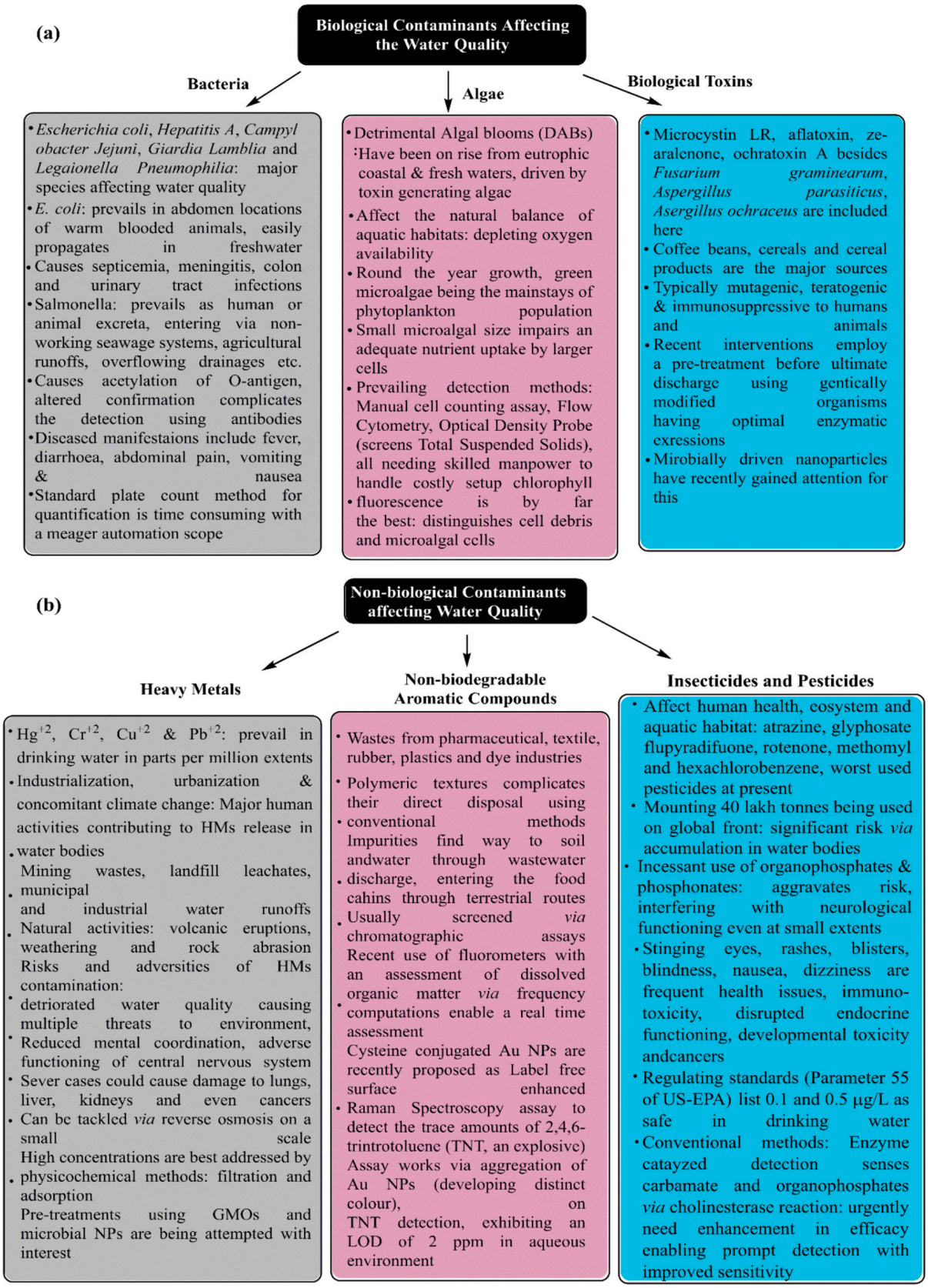

Fig. 2. (a) Major biological contaminants affecting the water quality, distinguished as bacteria, algae, and biological toxins, (b) Prominent non-biological contaminants affecting water quality, distinguished as heavy metals, insecticides and pesticides, and non-biodegradable aromatic compounds.

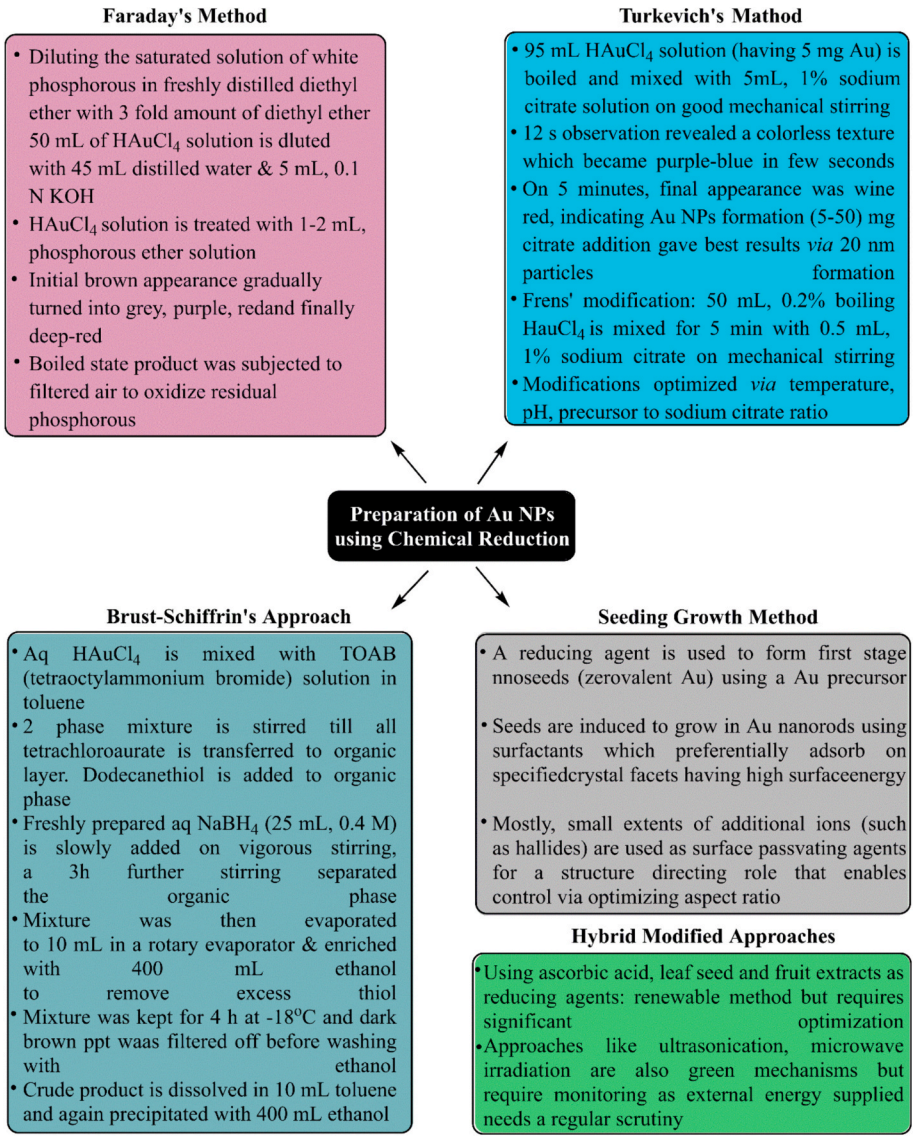

Fig. 3. Salient aspects of prominent chemical reduction methods for preparing Au nanoparticles, varying precursor to reducing agent stoichiometry is the basis of altered morphology and diversified applications.

electronic properties. Smaller dimensions attribute to a low energy band gap, owing to which, electrons from valence band are easily transitioned to conduction bands, generating the exciton promptly. The working mechanism for controlling the size and shape of NPs, is the optimized precursor to reducing agent stoichiometry, wherein rod or spherical morphology could be obtained. Other than precursor to reducing agent ratio, working pH, temperature and the precursor type are the prominent factors affecting the pace of NPs formation. From the precursor viewpoint, oxides are most easily reduced while nitrates are relatively tough to treat. With reference to pH and temperature, the optimum responses are generally retrieved for physiological pH and temperature albeit there may be variations for chemical methods. A number of iterations for size and morphology control of Au NPs *via* varied precursor and reducing agent ratios, have been comprehensively discussed in the publications on Turkevich's method and its optimizations [77–79].

Keeping such performance regulating attributes of Au NPs in mind, the next section discusses about the last ten year studies on Au NPs biosensors monitored quality of water resources.

4. Recent studies on gold nanoparticles monitored water quality

As discussed in earlier sections, preferential use of Au NPs and corresponding assemblies in biosensing (environmental and health concerns, majorly) is due to their high native stability, enabling multiple functionalization abilities. Our cautious literature search consolidated Au NPs as sensing probes, *via* (i) aggregation based singular or combined use, (ii) engineered electrodes as sensing platforms, (iii) functionalization with peptides, amino-acids, antibodies or manifold enzyme-conjugated biomolecules (DNA or RNAzymes), (iv) anchoring over graphene and reduced graphene assemblies, and (v) a miscellaneous approach (comprising integration of two or more of first four principles. The separate listing of graphene or graphene oxide conjugated Au NPs as functionalization assays is due to chemically distinct nature of graphene from the biological entities (proteins, antibodies and others). The surface versatility and tuneable energy levels of graphene makes it unique for engineered optoelectronic responses *via* numerous functionalization routes encompassed enhanced interactions for industrial, biological and energy harvesting [89,90].

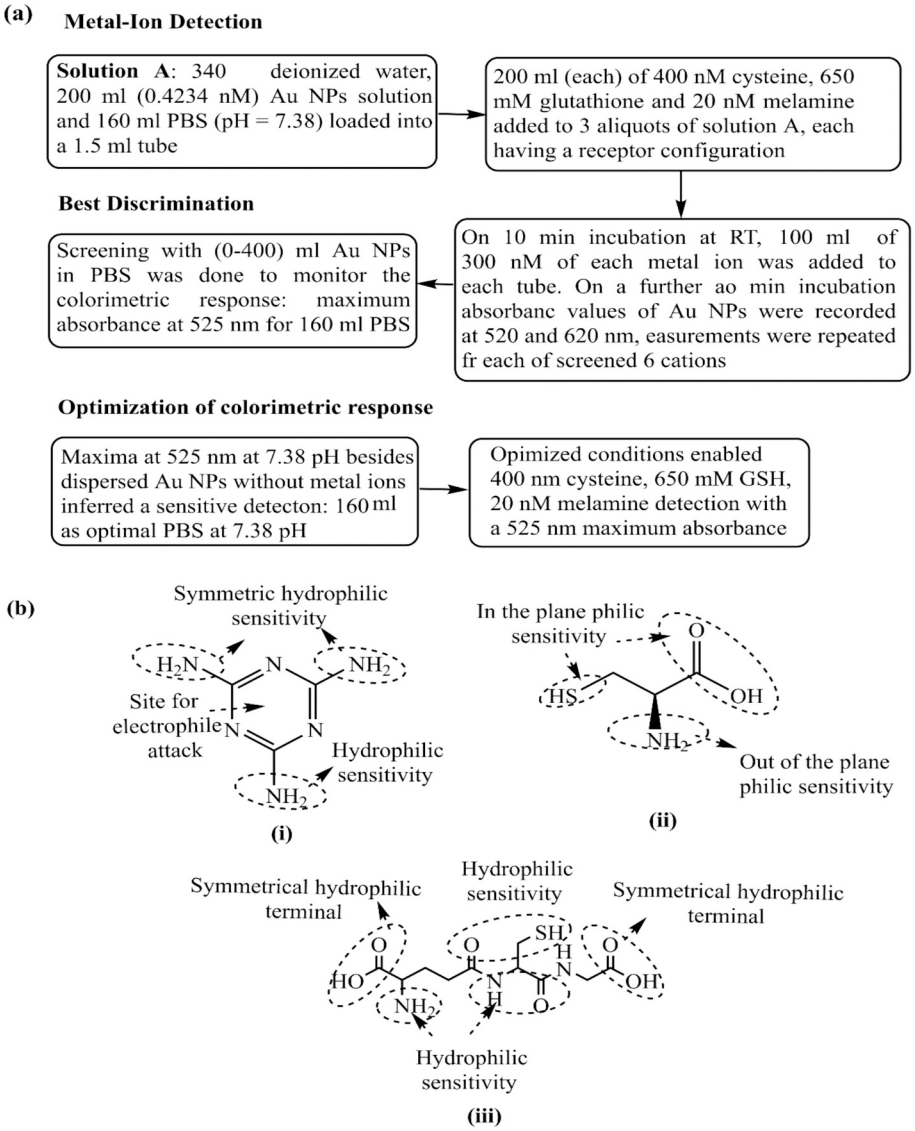

Fig. 4. (a) Metal ion detection and colorimetric response optimization steps for the 2019 study by *Li and colleagues* [95], (b) Molecular structures of (i) melamine, (ii) cysteine, and (iii) glutathione, with plentiful –OH, -SH and $–NH_2$ functional groups conferring a hydrophilic sensitivity. This implies that detection of these moieties mandates the probe interaction *via* hydrogen bonding, philic-philic or philicphobic interaction forces.

4.1. Aggregation facilitated singular or combinatorial assays

This section comprises the studies monitoring water quality *via* singular and combined (with other metal/metal oxide NPs) use of Au NPs. Working principle herein, uses distinct optical properties of monodispersed and aggregated states, the latter resulting in diminished energy due to increased sizes and reduced QC. So, the screened stimulus is detected *via* changes in native SPR of Au NPs through modulated dispersion regimes. The observed SPR of Au NPs varies as per the capping agent interaction with underlying NPs. Irrespective of formation mechanism, the SPR is observed corresponding to 520 nm, a variation arises due to distinct dispersion interception in course of UV–Vis spectroscopy [91]. The morphologies and architectures of NPs are the riders of their sensing abilities due to varied QC extents. For instance, a number of studies employ combinative use of NPs whereby the participation of capping layer is reduced to bare minimal. Regarding the morphology specific distinctions, the rod regime is better suited for sensing applications due to its capability of screening multiple functional responses on the same surface simultaneously. For instance, carbon nanotubes functionalized with Au NPs-anchored enzymes have been significantly explored as corresponding substrate detection(s) assemblies. Such distinctions are not feasible with spherical NPs which are better suited for adsorption, drug loading and charge transfer driven transport and surface engineering needs. The core-shell architecture is a characteristic configuration of NPs whereby enhanced protection, encapsulation extent and controlled release could be achieved *via* surrounding the functional NPs with a compatible shell. The functional aspects of shell material include a high dispersibility, biofunctionalization ability and control of optical properties. The uniqueness of these NPs pertains to their core-shell organic and inorganic sensitivity, with sizes in the order of few μm. These heterogeneous arrangements are highly stable in ambient conditions (at <200 °C) with minimal oxidation in (200–400)^{o}C. Unlike the conventional NPs, the specific characterizations for core-shell NPs are aberration corrected scanning tunnelling electron microscopy (equipped with high angle annular dark field detector), energy-dispersive X-ray spectrometry, electron energy loss spectroscopy. The shell protection in makes these NPs as highly useful for biomedical applications (bioimaging, drug delivery, sensing and gene delivery) [92–93].

Exploiting such remarkable attributes of core-shell morphology, a

2017 study by *Dong and colleagues* [94] developed Ag (core) and Au (shell) containing NPs which were conjugated with iridium (III) complex to screen cyanide presence in the water samples. The mechanism involved luminescence monitoring, getting quenched on (Ir(7-chloro-2-phenylquinoline)$_2$(4,7-dimethoxy-1,10-phenanthroline) (complex I) adsorption over Au surface of Ag@Au NPs. Electrostatic interactions between cationic, (Ir(7-chloro-2-phenylquinoline)$_2$(4,7-dimethoxy-1,10-phenanthroline) and Au shell, stabilized the assembly. The source of quenching was energy transfer from Ag@Au NPs to complex I *via* (300–800) nm absorption over Ag NPs. Such binding force dynamics engineered resonance of core-shell NPs and complex I- luminescence. Cyanide screening was facilitated by restoration on loss of Au shell, with Ag core being unable to do so. Inspection revealed a high sensitivity with 0.036 μM LOD with null detection of 10 fold contents of erstwhile anions. The approach could be extended to CN^- similar impurities *via* interacting with complex I. The optimized functioning of designed Au—Ag comprising core-shell NPs draws considerable interest wherein Au NPs as shell attributed to a flexible geometry and topology with low reactivity of Ag NPs containing core. Such an integrated assembly enabled thermal and oxidative stability of core NMs, making them suitable for biomedical, electrical and semiconducting applications. Thus, Au NPs as shell, conferred protection to Ag core and engineered a precise stimulus detection.

Subsequent 2019 effort used a colorimetric assay comprising cysteine, L-glutathione and melamine as recognition entities for screening toxic metal ions. Binding affinities of toxic cations with these recognition receptors were screened *via* Au NPs aggregation and consequent colorimetric response. The optimized configuration achieved significant Ti^{4+}, Cr^{3+}, Mn^{2+}, Fe^{3+}, Pb^{2+} and Sn^{4+} discrimination, in deionized water (DW) and real samples. Fig. 4a illustrates the detection procedure optimization for this study wherein, selective response was monitored *via* screening the absorption with and without Ti^{4+}, Cr^{3+}, Mn^{2+}, Fe^{3+}, Pb^{2+}, Sn^{4+} bound state of Au NPs at (300–1000,5000,10,000) nM. Six parallel measurements were made for each cation, generating a matrix of 6 ions, 3 receptors and 6 replicates. Thereafter, LDA (Linear Discriminant Analysis) converted this matrix into canonical factors, generating 3D-plots, with 95% confidence. The LDA scores for each cation revealed distinct clustering and discrimination. Analysis for intuitive distribution revealed a possible prominence in 300–10,000 nM range, exhibiting Ti^{4+}, Cr^{3+}, Sn^{4+}, Mn^{2+}, Pb^{2+} as preferentially captured by cysteine and melamine. Lower Au NPs absorbance differences with and without cations inferred a moderate receptor binding, with strongest affinity for cysteine. The discrimination accuracy (DA) were 75% (cysteine), 72.2% (glutathione), 72.2% (melamine), 94.4% (cysteine-glutathione), 91.7% (melamine-glutathione) and 91.7% (melamine-cysteine) and 100% (cysteine-glutathione-melamine), signifying a synergistic response.

Fig. 4b depicts melamine, cysteine and glutathione structural distinctions, wherein plentiful –OH, =O and –NH_2 functionalities exhibit a hydrophilic sensitivity. While glutathione is a physiological antioxidant, melamine is a toxic molecule with an excessive use being prohibited by FDA. The quantitative performance of developed probe was monitored using (100−1000) nM cationic extents, at 100 nM intervals. Maximum response was ascertained for 800 nM Ti^{4+}, 800 nm Cr^{3+}, 200 nM (each for) Mn^{2+}, Pb^{2+}, Sn^{4+} and 400 nM Fe^{3+}. The sensor array demonstrated nM sensitivity for Ti^{4+}, Cr^{3+}, Mn^{2+}, Fe^{3+}, Pb^{2+}, Sn^{4+}, with (100–900) nM linear responses for Ti^{4+}, Cr^{3+}, Mn^{2}, Pb^{2+}, (100–800) nM for Fe^{3+} and (100–1000) nM for Sn^{4+}. A linear variance of dose-response curve inferred stable cation-recognition receptor interactions with discrimination analysis revealing (Ti^{4+}-Mn^{2+}), (Ti^{4+}-Mn^{2+}-Sn^{4+}) and (Ti^{4+}-Cr^{3+}-Mn^{2+}-Sn^{4+}) for 1:9, (2:8, 3:7, 4:6, 1:1, 6:4, 7:3,8:2, 9:1), (2:2:6, 2:6:2, 6:2:2, 4:4:2, 4:2:4, 2:4:4) and (2:2:2:3, 2:3:3:2, 2:2:2:3, 3:2:2:3, 3:3:2:2, 3:2:3:3) stoichiometries, facilitating a 300 nM detection. Analysis of real water samples from *Yuyuantan Park* in Beijing, revealed no ion detection by ICP-MS but on being spiked at 300 nM to the sensor array, the screened ions were distinguished. Identification for screened

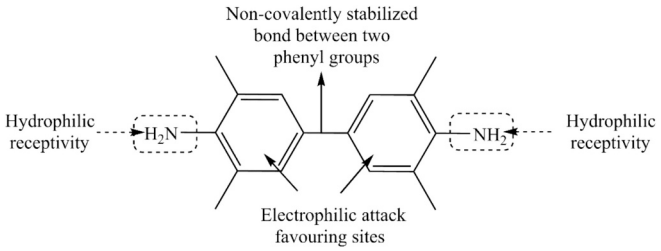

Fig. 5. Molecular structure of 3,3′,5,5'tetramethylbenzidine (TMB), the –NH_2 substituted phenyl rings confer a moderate interaction with Au NPs functionalized MOF framework. No steric hindrance in the –NH_2 groups vicinity argues well for their probing involvement. The (50–200) nM linear detection range with 8.1 ng•mL^{-1} LOD and (106–110)% recovery rate in 2019 study by *Li and colleagues*, creating interest for possible structural similarities with screened ampicillin, tetracycline and oxytetracycline [96].

cations was also made on serum samples, revealing a unique response alongwith LDA assisted six samples being clustered as distinct groups [95]. The working principle could be used to estimate the chemically similar impurities (similar group elements from periodic table), illustrating usefulness *via* characteristic Au NPs aggregation encompassed distinctive optical responses.

The next 2019 effort was the study by *Li and colleagues* [96] who screened antibiotics contaminated water samples using metal organic framework (MOF) conjugated aptamer functionalized with 3,3′,5,5'tetramethylbenzidine (TMB)-H_2O_2. The assay monitored TMB catalytic oxidation (included as label) from colourless to blue, using aptamer as antibiotic recognizer, *via* ascertaining the variations in MOFs catalytic activity. Out of Fe-MIL-53, Fe-MIL-88 A and Fe-MIL-100 ligands, Fe-MIL-53 was chosen due to its superior topological flexibility and small electron transfer impedance. Working configuration comprised quenched MOF catalysis through antibiotic-Au NPs-aptamer conjugate coating on MOF outer surface, increasing the impedance *via* reduced electron transfer. Selectivity and sensitivity of the assay revealed a (50–200) nM linear detection with 8.1 ng•mL^{-1} LOD and (106–110)% recovery, exhibiting suitability for chloramphenicol detection besides viable potential for ampicillin, tetracycline and oxytetracycline screening. Fig. 5 depicts TMB structure wherein –NH_2 substituted phenyl rings manifest a hydrophilic likability with an electrophilic proximity of π-conjugation rich phenyl rings. Development of such probes argued variability for a feasibility to screen hydrophilic contaminants. One concern shared by the authors though, points to 8.1 ng•mL^{-1} LOD, unable to screen fewer extents. A feasible extension of the work could be the SPR variations of Au NPs alone and their compatibility with Ag, Cu, Co, Mn for consolidated probe configuration to screen water-borne pathogens.

Next in line is a 2021 study wherein Au NPs functioned as segmented bridge for growing Ag shell and gather together the Au-Fe_3O_4 NPs with a dumb-bell morphology exhibiting a magnetic sensitivity. The assembly was optimized to screen aflatoxin *via* modulating the transverse relaxation time of examined water molecules. The Ag@Au-Fe_3O_4 nanoscale assembly was controlled *via* H_2O_2 which on horseradish peroxidase degradation, reduced Ag^+ to Ag^0, accompanied with transformation of dispersed Au-Fe_3O_4 NPs to Ag@Au-Fe_3O_4 aggregated entities. Detection sensitivity of assay was 3.81 pg•mL^{-1}, on par with competitive immunoreactions, improving the ELISA and HPLC screening by 21 and 9 folds [97].

A nearly similar but recent study used Au@MnO_2 core-shell morphology to screen *E. coli* contamination *via* accessing β-galactosidase action on single particle enumeration *via* colour code distinction. Presence of *E. coli* in tested water stream hydrolyzed *p*-aminophenyl β-D-galactopyranoside to p-aminophenol (AP) *via* endogenous β-galactosidase. Detection was confirmed *via* MnO_2 shell-AP reaction, resulting in blue shift of localized SPR (bright yellow to green colour change) with

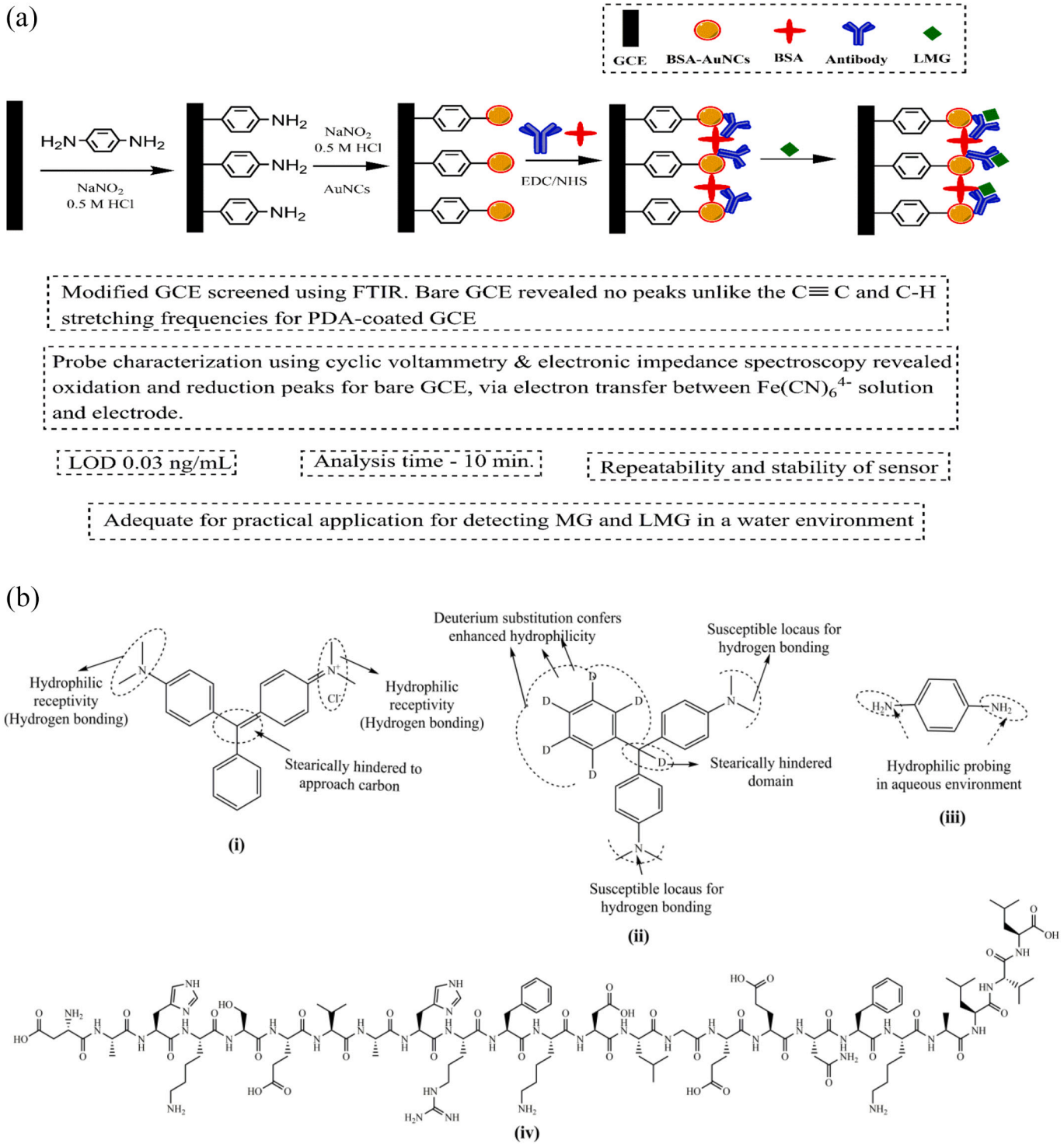

Fig. 6. (a) Optimization of probe assembly *via* N,N′-(3-dimethylaminopropyl ethylcarbodiimide hydrochloride) EDC-NHS (N-hydroxysuccinimide) assisted chemical reaction and the subsequent validation *via* cyclic voltammetry and electrical impedance spectroscopy for the 2016 study by *Zhu and colleagues* [101], (b) Characteristic hydrophilic and hydrophobic functionalities of (i) Malachite green (MG), (ii) Leucomalachite green (LMG), (iii) 1,4-phenylenediamine (PDA) and (iv) Bovine serum albumin (BSA), pertaining to the discussion of 2016 study by *Zhu and associates*. The matching of distributive hydrophilicities amongst PDA, BSA and MG, LMG offer enhanced understanding of probe design for distinctive MG and LMG recognition.

concomitant Mn^{+2} formation. The assay exhibited an LOD of 15 CFU•mL^{-1} over a (100–2900) CFU•mL^{-1} dynamic range, enabling an ultrasensitive and economic *E. coli* screening in river water. The robust configuration with dynamic working feasibility of the probe demonstrated the assembly as ultrasensitive, low cost measure to screen other than *E. coli* bacterial contaminations in river water and food samples [98]. Comparative analysis of last two studies [97,98] conceptualizes a wide anticipation of Au NPs comprising biosensors, *via* compatibility with Fe_3O_4 as well as MnO_2 and providing ultrasensitive detection of distinct contaminants. Such prospects illustrate the multifunctional analytical perceptivity of Au NPs with immense scope of modulated energy levels.

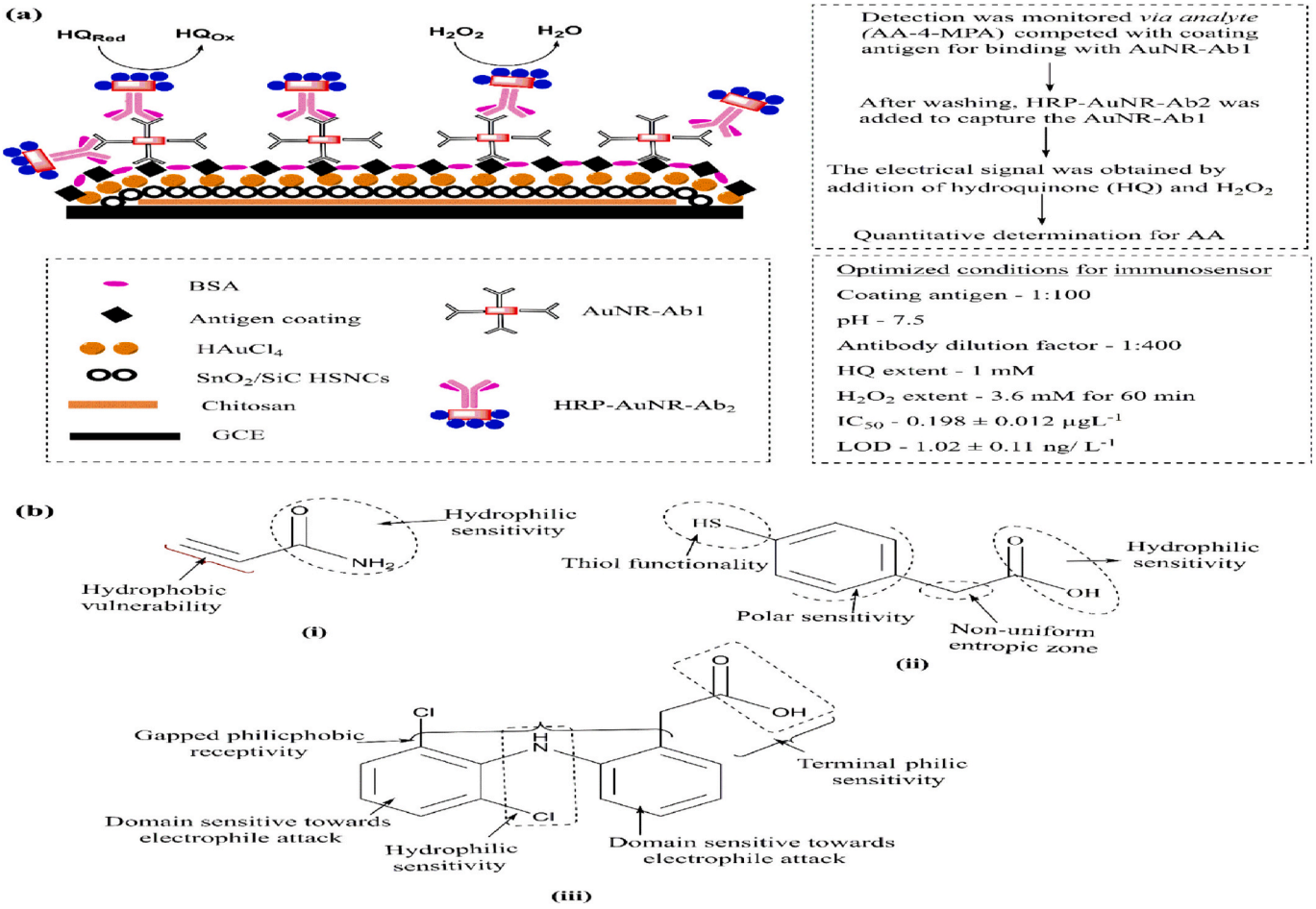

Fig. 7. (a) Schematic representation ofpH, dilution factor and H_2O_2extent driven detection methodology using Au nanorods conjugated with hollow SnO2-*SiC* spherical nanochains on chitosan pre-coated glassy carbon electrode, (b) Molecular structures of (i) acryalamide and (ii) 4-mercaptophenylacetic acid, and (iii) diclofeanc, with –NH, Cl, and –COOH and pi-conjugation conferring phenyl rings confer a distributed philicphobic receptivity. The structures pertain to the screened impurities in food and water samples in the 2018 study by *Wu and colleagues* [102].

Another worthwhile effort from 2021 optimized a surface-enhanced Raman Scattering (SERS) coupled wavenumber selection chemical signal monitored approach for screening Hg^{+2} in aqueous environment. Optimized probe configuration involved Au@Ag core-shell NPs which were used as SERS substrates while rhodamine 6G (R6G) was included as Hg^{+2} signaling probe. The Au NPs were prepared *via* 30 min uninterrupted stirring of 50 mL, 0.25 mM $HAuCl_4$ and 750 μL, 1% $C_6H_5Na_3O_7•2H_2O$ mixture at boiling conditions. Henceforth, 2 mL, 1% $C_6H_5Na_3O_7•2H_2O$ was added again to the reaction mixture. Finally, to develop Ag NPs shell, 9 mL, 1 mM $AgNO_3$ was injected at the rate of two drops per minute, followed by another 30 min stirring to obtain Au@Ag NPs. Physical indication of NPs formation was red wine to orange-yellow conversion. Characterization of as formed NPs corroborated their nanoscale traits, with 28.51 nm as average hydrodynamic diameters (using DLS), a spherical morphology (*via* TEM) and an SPR peak within (388–498) nm alongside a face-centred cubic, crystalline texture. The Hg^{+2} screening by optimized probe was accomplished *via* quenching of R6G strong SERS signal due to its interaction with Au@Ag NPs, resulting in progressive replacement of Ag^{+} by the bound Hg^{+2}. Enhanced extents of bound Hg^{+2} within $(10^{3}–10^{-2})$ μg•g^{-1} resulted in disorganized Ag shell morphology in the TEM micrographs of the probe, revealing an aggregated state. Correspondingly, a blue shift in UV–Vis SPR peak of Ag shell of Au@Ag NPs was noticed, reducing Hg^{+2} to Hg^{0} on the Ag shell surface of Au@Ag NPs, following Hg^{+2}-citrate ion of Au@Ag NPs complex formation. The SERS coupled sensing revealed a good efficacy over the SPR methodology, developing 0.9745 and 0.9773 as correlation coefficients within $(10^{2}–10^{-3})$ μg•g^{-1}. Specificity analysis of probe for 1 μg•g^{-1} Hg^{+2} with and without 100 μg•g^{-1} Ba^{+2}, Ca^{+2}, Cd^{+2}, Co^{+2}, Cu^{+2}, Fe^{+2}, Fe^{+3}, Mg^{+2}, Mn^{+2}, Ni^{+2}, Pb^{+2} and Zn^{+2} revealed Hg^{+2} acceptable SERS signal, inferring a good sensitivity. The recovery (88.45–94.73)% and (3.28–5.76)% coefficient of variations revealed a suitability of optimized SERS modulation for Hg^{2+} screening in aqueous conditions [99].

Summarizing the findings of singular or combined state Au NPs prevalence mediated SPR varied sensing responses, reveals a high sensitivity, reproducibility and specificity of various contaminants in examined water samples. There seems a possibility of still higher accuracies being accomplished *via* optimum combinatorial approaches whereby detection precision and reproducibility could be improvised. The accuracy of responses is sharply affected by the respective preparation methods of NPs with a higher reliability of chemical approaches.

4.2. *Use of Au nanoparticles modified electrodes as sensing platforms*

This section comprises the studies where Au nanothin layers functionalized electrodes (electrochemical detection) have been used as sensing platforms. A high electrical conductivity of Au augments its electrochemical abilities, paving way for accurate and precise stimulus detection [100]. Added incentive herewith is the robust size-shape modulation of Au NPs whereby detection platform geometry could be modulated. Herein, many studies have demonstrated thin film monodispersed textures of Au NPs in combination with other elements (such

as zirconium, vanadium *etc.*) for improved responses. A serious challenge in such probe configuration is the rigorous characterization *vis-à-vis* stimulus nature and intensity. The working principle screens the probe electrical and optoelectronic response in varying environments. Ahead is the discussion of post 2015 studies in this regard.

The 2016 attempt by *Zhu and associates* [101] reported a sensitive electrochemical impedance spectroscopy (EIS) assay for malachite green (MG) and leucomalachite green (LMG) detection using bovine serum albumin-functionalized Au nanocluster (BSA-Au NC) Ab composite film conjugated immunosensor. The investigators modified GCE with 1,4-phenylenediamine (PDA, for $–NH_2$ group), to obtain a stable surface suited for covalent binding. Fig. 6a summarizes the optimized probe configuration *via* EDC (N,N′-(3-dimethylaminopropyl ethylcarbodiimide hydrochloride))-NHS (N-hydroxysuccinimide) conjugation and its validation *via* cyclic voltammetry (C*V*) and EIS scrutiny. Analysis revealed an agreement for circuit model over the scanned frequencies with negligible resistance R_s (95 Ω) and impedance variations Z_w (1.45 m Mho) for each impedance scan, inferring no electrode surface modification. Owing to this, R_{et} was chosen for interfacial properties, increment in which deciphered electrically insulated LMG and Ab interactions. The analysis efficacy varied with incubation time and solution pH, examined *via* Ab-modified electrode immersion in LMG solution (10 ng•mL^{-1}) at (6–8.5) pH for (10–60) min. For calibration curve and interaction specificity, the EIS response to LMG concentrations was investigated at 5 mV, (0.1 Hz-100 KHz) and 0.29 V. The R_{et} increased with increasing LMG extents, supported by relative resistance and calibration curve linearity within (0.1–10.0) ng•mL^{-1}. With a 0.03 ng•mL^{-1} LOD, the R_{et} change was steady at >10 ng•mL^{-1} LMG. The EIS repeatability for 10 ng•mL^{-1} LMG with five assessments deciphered a 5.6% relative standard deviation (RSD) at 4 °C. Till 2 weeks, no significant reduction was noticed and impedance remained 90% of initial extent. Commercial feasibility was determined *via* EIS and ELISA inspections of (1–5) ng•mL^{-1} LMG spiked farm water samples. Analysis revealed good recoveries and EIS precision on comparative assessments with ELISA and Mass spectroscopy estimations, demonstrating suitability for aqueous MG and LMG screening. Fig. 6b depicts MG (i), LMG (ii), 1,4-PDA (iii) and BSA (iv) structural distinctions, wherein hydrophilic proximity favours 1,4-PDA coated BSA-Au NC constituted electrodes. The hydrophilicity of BSA argues well for its functionalization with Au-BSA NCs. Distinct binding accuracies with detection thresholds for MG and LMG were due to higher LMG hydrophilicity as it is substituted with five deuterium atoms. The structural distinctions of LMG and MG also provide a clue for the LOD dissimilarities as exposed hydrophilicity of LMG seems readily accessible by Au-BSA NC hydrophilic sensitivity. These attributes could be conceptualized for probe configurations *via* structure-activity-relationships modulations.

Subsequent attempt on Au NPs monitored water quality used high SA, hollow SnO_2-*SiC* spherical nanochains and Au nanorods (NRs), anchored on a chitosan pre-coated GCE for acrylamide (AA) screening in water and food samples. The 50 nm long, 20 nm wide Au NRs were prepared *via* seed mediated mechanism, using $HAuCl_4$ as precursor, $NaBH_4$ as reducing agent and CTAB as capping agent. The coating antigen, AA-4-mercaptophenylacetic acid-ovalbumin conjugate (AA-4-MPA-O*V*A) was immobilized on electrode while AA-4-MPA specific polyclonal Ab was conjugated to Au NR as primary antibody (AuNR-Ab_1). The Horseradish peroxidase labelled anti-rabbit Ab goat was conjugated to Au NRs as secondary antibody (HRP-AuNR-Ab_2). Sensing configuration involved dropping 5 μL, 0.2% chitosan solution over the electrode and RT drying. Subsequently, 0.5 mg SnO_2-*SiC* HSNC was monodispersed in 1 mL DW followed by its 5 μL-deposition on chitosan coated electrode, and a second RT drying. Thereafter, electrochemical deposition was done in 4 mL, 0.5 mM $HAuCl_4$ *via* (−0.3 to 0.3) V ranged CV for 5 cycles at 50 mV•s^{-1}. Fig. 7(a) summarizes the detection methodology optimization for validated pH, dilution factor and H_2O_2 extents. Real analysis on drinking water, coffee and potato chips revealed (45.9 ± 2.7) ng•kg^{-1} as LOD for (187 ± 12.3) ng•kg^{-1} to (104 ± 8.2) μg•kg^{-1} linear range. The AA content was ascertained as 1000 fold higher for coffee and potato chip, ruling out LOD quantification. Distinguishing aspects comprised stability monitoring *via* 4 °C periodic current response time assessments, revealing 97.3, 93.6, 90.7% initial current retaining on one, three and six weeks. Likewise, electrode regeneration monitoring revealed (15–50)% reduced output with no reuse feasibility, due to varied pH triggered electrode surface tampering. The AA recoveries ranged (86–115)% with (6.4–8.6)% variation coefficients, and (86.5–112), (4.3–9)% extents for coffee and potato chips. Selectivity analysis for AA-4-MPA revealed no cross-reactivity to 4-MPA, 4-aminothiophenol, AA, methacrylamide, methyl acrylate and acrylic acid [102]. The $–CO-NH_2$, –COOH, -HS functionalities of AA and 4-MPA exhibit compatibility whereby 4-MPA as electrode coating agent attributed well for immobilized Au NRs, vide interfacing thiol linkage (Fig. 7(b)). A pertinent concern herewith is the inadvertent AA use in childcare products (talc, soaps *etc.*), accounting for its recent suspension by US-FDA.

A recent investigation by *Iqbal and colleagues* [103] used DNA aptamer conjugated magnetic beads to quantify the *C. parvum* oocysts, frequent contaminants in potable water. A sensitive 3′-biotinylated R4–6 aptamer was used as secondary ligand for immobilizing streptavidin coated magnetic beads. The ligand bound magnetic bead assembly was then included within Au NPs modified screen printed carbon electrode (SPCE). The detection efficacy for *C. parvum* oocysts inferred specificity using square wave voltammetry with no *Giardia duodenalis* cysts binding, another ubiquitous water-borne pathogen. The sensing LOD was ascertained as 50 units with steadfast *C. parvum* oocyst detection in raw lake and river water. The study also screened a combination of Au NPs coated carbon electrode and aptasensor functionalized magnetic beads for deleterious aqueous contaminants, revealing significance *via* manifold Au NPs morphologies. The subsequent attempt was a 2019 study by *Costa-Rama and colleagues* [104], wherein a paper-based platform was used to screen diclofenac (DCF, an anti-inflammatory drug) in contaminated water samples. Carbon-ink paper was used as working electrode and two metallic wires, linked *via* Au connectors functioned as reference and counter electrodes. Porous paper membrane aided the sample preconcentration apart from its de-coupling and detection, accomplishing a 60 folds enhanced sensitivity and 8000 fold lower LOD over the DCF pre-concentration on the working electrodes. The detectable adsorption attributed to (0.10–5) μM and (5–100) μM linear detection. Feasibility for DCF contamination in spiked tap water samples revealed a 70 nM LOD with 5% RSD accuracy. Structural versatility of probe aided in integrated assembly of eight electrochemical cells, with -NH, Cl, and -COOH functionalities inferring an aqueous persistence besides π-conjugation supported electrophilic receptivity (Fig. 7biii). The cationic probes efficiently immobilized and detached the drug. It is essential hereby to understand the mitigating philicphobic sensitivities in such assays, necessitating a modulation of philicphobic force gradients is needed, could be accomplished *via* computational techniques ascertained most stabilized combination with least binding energy.

A latest attempt herein used Au NPs-PPy (polypyrrole)-$Ti_3C_2T_x$ (titanium carbide) nanocomposite, prepared *via* robust layer by layer self-assembly. Probe analysis using XPS and XRD revealed $Ti_3C_2T_x$ (a natural 2D material consisting of layered nitrides) significance in the formation and alignment of PPy (an organic polymer derived from pyrrole oxidative polymerization) besides Au NPs growth. Screening of composite texture revealed enhanced stability with improved electrochemical performance wherein Au NPs conferred the ability to form covalent bonds with biomaterials *via* Au—S linkage. Sensing response of optimized assembly for Pb^{+2} detection revealed a $5•10^{-14}$- $1•10^{-8}$ M linear working range with $1•10^{-14}$ M LOD. Besides the probe exhibited good selectivity and sensitivity for Pb^{+2} screening in environmental fluids (Nong Fu spring and tap water) [105]. Another significant effort from 2023 itself demonstrated an integrated nanoscale configuration of an electrochemical biosensor wherein functional probe design comprised a

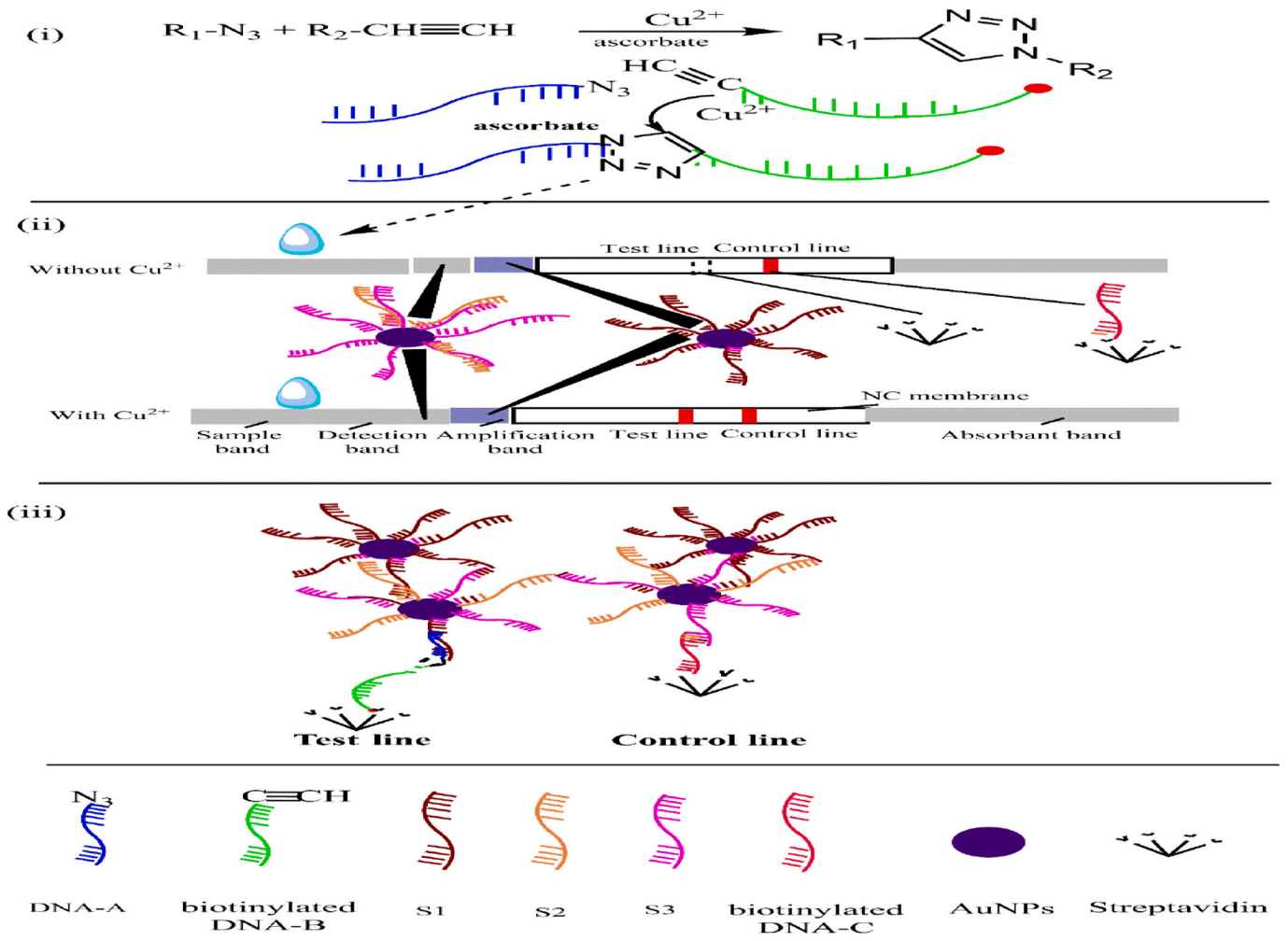

Fig. 8. Representative aspects of (a) Lateral flow test strip (SA-LFTS), (*Wang and colleagues* 2017), (i) Cu^{+2} detection based on Cu^{+}-catalyzed click chemistry, (ii) Visual detection of generated click-ligated ssDNA product, SA-LFTS includes an additional amplification pad (compared with traditional LFTS) that confers higher sensitivity [108]. The streptavidin-biotin interaction at the test line allows an easier implementation of the test, and (iii) The test and control lines of SA-LFTS assay after flow with Cu^{+2} addition. Au NPs are captured *via* streptavidin-biotin interaction and ssDNA hybridization.

carbon nanotubes-Au NPs and *E. coli*-polyclonal Ab and BSA engineered glassy carbon electrode (GCE), immersed in 0.1 M phosphate buffered saline (pH = 7). The sensor worked *via* acetaminophen (a non-opoid analgesic and antipyretic drug used to treat pain and fever) conjugation, detecting *E. coli* aqueous contamination *via* conductivity and current variations. Precision of the working assay was screened using square-wave, differential pulse and cyclic voltammetry, deciphering an LOD of 3.02 CFU•mL^{-1} *E. coli* detection in 3 min with reasonable accuracy, specificity, repeatability and reproducibility. Since *E. coli* is a frequent invader of food and drinking water, the demonstrated sensor configuration provides vital clues to integrate nanostructures for their synergistic bio-electronic response [106]. Thus, a generalized assessment of the studies in this section infers that Au NPs coating over the GCE surface either as nanothin films or *via* nanocomposite texture, efficiently screens aqueous contaminants with low response times. Indeed, probe functioning do requires a rigorous optimization as is the electrode stability for repeatable accuracies.

4.3. Biomolecules functionalized Au nanoparticles as water quality monitoring probes

This section comprises biomolecules (such as antibodies, enzymes, peptides, aptamers, engineered oligonucleotides *etc.*) functionalized Au NPs as water quality sensing probes. Select ligands or surface pre-treatments used *via* Au NPs functionalization herein comprise alkane thiol conjugation, Ab linking *via* avidin-biotin mutual interception, biocompatible peptide-dye conjugation and combinatorial regimen with other conducting/semi-conducting materials. Functionalization method needs a rigorous monitoring to ensure minimal interactions failing which, the probe's working efficacy could be tampered with.

The first major post 2015 effort herein used oligonucleotide functionalized Au NPs for rapid and specific *Staphylococcus aureus* (*S. aureus*) detection using a colorimetric mechanism. The probe configuration involved functionalization of a chemically modified 11-mer sequence onto the Au NPs *via* chemical conjugation. Analysis revealed Au NPs aggregation in response to *S. aureus* detection (as supernatants). The designed Au NPs-oligonucleotide assembly exhibited a biological suitability in creek and ocean water besides being storable as lyophilized powder, suggesting transportation and packaging robustness. Another advantage comprised the bacterial enzyme detection proximity (besides *S. aureus*) through modifications in oligonucletide array and coated NPs morphology. It is pertinent to mention here that *S. aureus* is a Gram-positive bacterium with a spherical morphology familiarly prevailing in the upper respiratory tract and on skin. The bacterium is positive for catalase and NO_3^- reduction, ruling out a mandatory need of oxygen for growth. Opportune pathogenic expressions are widely manifested as common cause of skin infections (abscesses), respiratory infections (sinusitis) and food poisoning. Major cause of such pathogenic

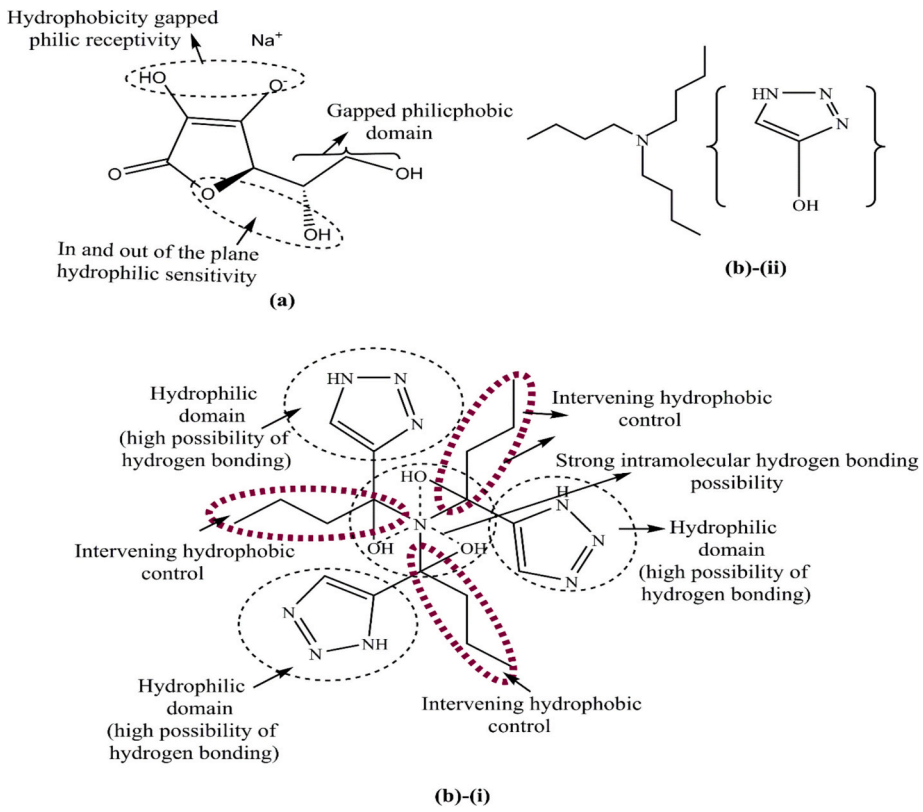

Fig. 9. Structural proximities of a) sodium ascorbate (SA), and (b)-(i) tris-(hydroxypropyltriazolylmethyl) amine (THPTA) and (ii) overlapping hydrophobic and hydrophilic domains in THPTA structure. While SA facilitated the reduction in the Cu^{+} catalyzedazide-alkyne cycloaddition and chemical ligation of alkyne and azide modified ssDNA, the intent of adding THPTA was to stabilize water-soluble copper(I) ligand exclusively used in copper(I)-catalyzed alkyne-azide cycloaddition.

expressions is the virulence factor generation, including protein toxins and cell-surface proteins binding for inactivating the antibodies [107].

Progressing to 2017, the first notable attempt by *Wang and colleagues* [108] demonstrated a signal-amplified lateral flow test strip (SA-LFTS) for Cu^{+2} aqueous screening using click chemistry based Cu^{+} hybridization of ssDNA. The alkyne and azide modified ssDNA perceived Cu^{+2} *via* Cu^{+} aided cycloaddition *vis-à-vis* alkyne and azide groups modified ssDNA, chemical ligation. The ssDNA-Au NPs hybridization resulted in high sensitivity with naked eye visualization of test strip ligated ssDNA. Primitive SA-LFTS features comprised DNA-A (azide group) and biotinylated DNA-B (alkyl group) as Cu^{+2} recognition reagents. Assay worked through azide cycloaddition and alkyne functionalized ssDNA to generate a click ligated, ssDNA chain (like, DNA-A-DNA-B). This ssDNA was biotinylated and applied to the test strip (Fig. 8(i & ii)). The reaction commenced with ssDNA-DNA-Au NPs probe I hybridization on strip detection pad (partially complementary to DNA-A). Upon test line migration of this complex, it was captured by strepdivin-biotin complex *via* Au NPs binding. The Au NPs binding with DNA-C was deciphered as red band on control line, confirming a proper functioning of test strip. Thereafter, DNA-Au NPs probe II was hybridized with DNA-Au NPs probe I on the amplification pad, resulting in Au NPs test line accumulation. Monitoring the test line colour change validated Cu^{+2} existence, based on which the quantitative screening was optimized using portable strip reader recorded relative intensity. Fig. 8(iii) illustrates the

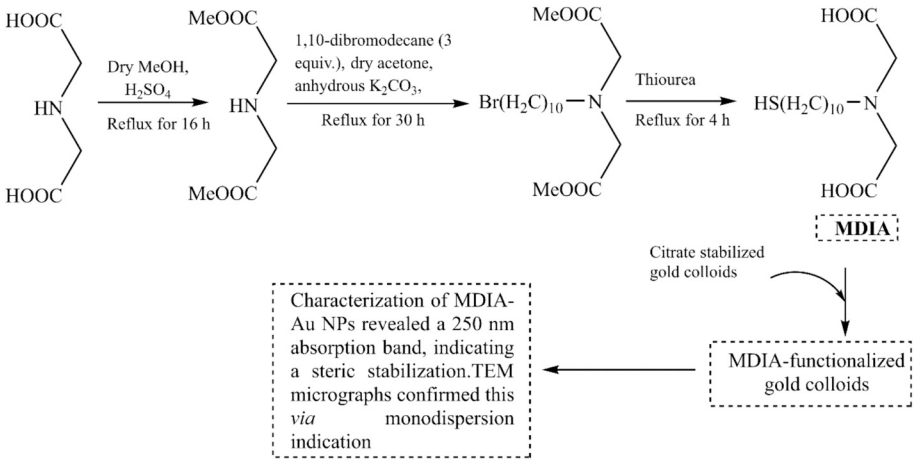

Fig. 10. Optimized procedure for 10-mercaptodecyl-1-iminodiacetic acid (MDIA) synthesis and its functionalization with Au nanoparticles, for the 2017 study by *Chai and colleagues* [110].

optimized probe configurations, wherein sodium ascrorbate moderated Cu^{+} catalyzed azide-alkyne cycloaddition and subsequent ligation of alkyne-azide modified ssDNA. The optical response for sodium ascorbate variations revealed 800 μM as adequate extent which was similarly ascertained as 1 mM for tris-(hydroxypropyltriazolylmethyl) amine (THPTA, for enhanced Cu^{+} binding) with a pH of 7 (highest relative intensity). Functional assay retrieved an LOD of 4.2 nM, ~four orders lower than US Environmental Protection Agency (EPA) prescribed 20 μM. Specificity for Cu^{+2} was monitored *via* test line colour intensity and Mg^{+2}, Hg^{+2}, Pb^{+2}, Ca^{+2}, Cd^{+2}, Zn^{+2}, Fe^{+3}, Na^{+}) responses. Except 100 nm Cu^{+2}, no ion developed a bright red band. Practical feasibility was studied using (20, 200 nM, 2 μM) Cu^{+2} spiked municipal and river water, retrieving (92.30–106.52)% recoveries, confirmed by inductively coupled Mass Spectroscopy (ICP-MS).

Fig. 9a depicts sodium ascorbate and THPTA distinctions, wherein oxygen, OH and Na^{+} functionalities of the former confer a hydrophilic sensitivity while the in and out O, –OH placements in the 5-membered ring and extended aliphatic chain manifested hydrophilicity. Similarly, the terminal –OH in aliphatic chain conferred philicphobic sensitivity. For THPTA, alternative hydrophilic and hydrophobic domains manifest a homogenization (Fig. 9b-i). The overlapping hydrophilic domains (-OH substituted pyrimidine ring) and N centred 3 alkyl chains (ACs) are demarcated in Fig. 9b-(ii). The THPTA inclusion in the probe assembly stabilized water-soluble Cu (I) ligand, widely used in Cu(I)-catalyzed alkyne-azide cycloaddition [109]. These logics could be extended to detection assays *vis-à-vis* moderate analyte-probe interactions. Stronger DNA-Au NPs hybridization with sodium citrate affirmed a best sensing, leaving aside PBS and Tris-HCl.

Another significant 2017 study from *Chai and colleagues* [110] used 10-mercaptodecyl-1-iminodiacetic acid (MDIA) to modify Au NPs for RT Cu^{+2} sensing from solution. Fig. 10 illustrates MDIA synthesis, its post synthesis characterization and Au NPs (made using Turkevich's method)-functionalization Subsequent to Cu^{+2} binding, the MDIA@Au NPs absorbance decreased with a distinct 560 nm band besides a red to purple change. These observations were complemented by TEM micrographs, exhibiting Cu^{+2}-carboxylate ligand complex formation on Au NPs surface with. The estimated LOD for Cu^{+2} was $1\bullet10^{-4}$ mol•L^{-1}, ascertained *via* colour change intensity. The 520 nm absorbance changes *via* calibration plot, revealed a linear trend for ($5\bullet10^{-6}$ to $5\bullet10^{-4}$) mol•l^{-1} Cu^{+2}. The 3.9% RSD for five assessments inferred reproducibility of the assay. The EDTA effect on MDIA@Au NPs *vis-a-vis* enhanced Cu^{+2} extents revealed sudden intensity increments *via* RT (610 to 520) nm blue shift, with red to purple colour change, indicating strong EDTA-Cu^{+2} interactions. The assay reusability screening revealed an aggregation (red to purple) on Cu^{+2} and EDTA addition. Continued EDTA addition generated red colour again, suggesting a reversible aggregation *via* metal ion chelation. The Cu^{+2} holding MDIA@Au NPs were thus, centrifuged to separate Cu^{+2} complex and the MDIA@Au NPs were dispersed in distilled water, promptly developing a red colour. Similar observations on equal Cu^{+2} addition to MDIA@Au NPs inferred the assay reusability. Analysis for Cu^{+2} detection from acidic waste having (30, 40, 50, 60 and 70) μM Cu^{+2}, was done *via* mixing 1 mL concentrated MDIA@Au NPs with 9 mL acid etching solution. On 30 min stirring, the mixture was centrifuged to retrieve the supernatant which on Atomic Absorption Spectrophotometer (AAS) screening, revealed 3051 mL•g^{-1} as absorption coefficient. Thus, this study used MDIA functionalized Au NPs to screen Cu^{+2} with a feasibility to screen erstwhile chelating agents other than EDTA.

Next in line is a 2018 study, using monoclonal antibodies (MAbs) and 6-carboxyfluoroscein labelled single stranded-thiol oligonucleotides (6-FAM-SH-ssDNAs) functionalized Au NPs. The study screened triazophos (a pesticide) *via* ovalabumin conjugated haptens competitive assay for antibodies anchored Au NPs. Functionalization with 6-FAM quenched the Au NPs fluorescence *via* inverse variance with analyte extent. Sensing parameters included an hour of salting whereby (166 ± 9) ss DNAs were loaded on Au NPs. Feasibility studies were done on water,

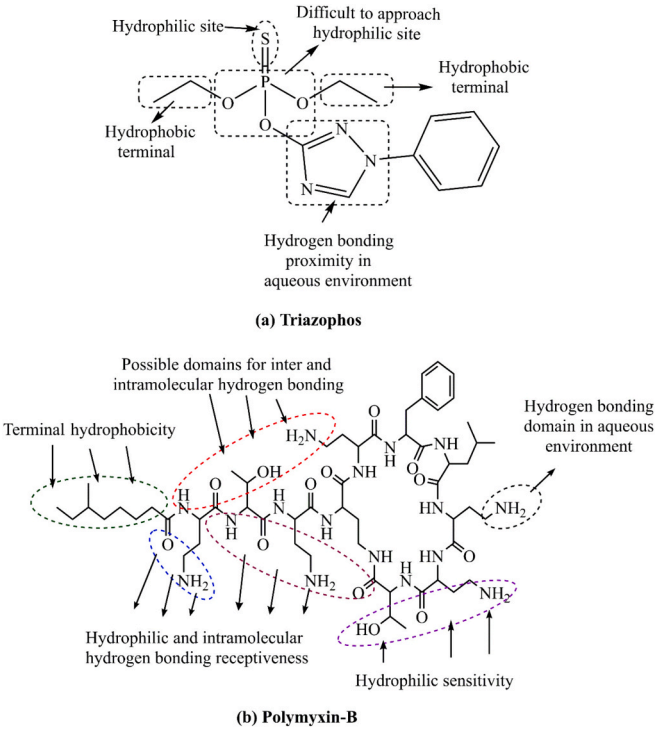

Fig. 11. (a) Distribution of hydrophilic and hydrophobic force factors in the insecticide triazophos, and (b) the drug polymyxin-B. Manifold hydrophilic sensitivities in both compounds confer the possibility of significant hydrogen bonding, with the latter exhibiting significant intra and inter molecular controls.

rice, cucumber, cabbage and apples, revealing (0.01–20) μg•L^{-1} linear range, 6 ng•L^{-1} LOD, (85–110.3)% recovery and (9.4–17.4)% RSD. The assay revealed 0.9794, 0.9758, 0.9783, 0.9841, 0.9709 correlations with liquid chromatography-tandem mass spectrometry (LC-MS) [111]. Specificity studies deciphered >2000 μg•l^{-1} IC_{50} for chlorpyrifos, chlorpyrifos methyl, parathion, malathion, diazonin and fenitrothion. The P and S double bond besides multiple N substituted 5-membered ring in traiazophos endow a tough biodegradation (Fig. 11a). Assay efficacy could be improved *via* S and P double bond interception, with 3 O linked to P and hydrophobic sensitivity at the terminal locations. The S atom in P—S linkage restricts the approachability to P *via* its lone pair electrons and reduces the hydrophilic activities of the pesticide. The π-conjugation at the terminal location of middle O atom linked to P manifests a electrophilic sensitivity and could be re-engineered *via* substitution to augment the detection *vis-à-vis* moderate cationic probe sensitivity.

The first noted attempt from 2019 used polymyxin-B conjugated Au NPs (PMB-Au NPs) for lipopolysaccharide (LPS) (a bacterial endotoxin) detection. Sensing probe comprised a U-bent fibre optic probe (UFOP), entrapping LPS from aqueous solutions using biomimetic self-assembled octadecyltrichlorosilanes (OTS) layer functionalization. Fig. 12 summarizes the UFOP fabrication and its characterization for sensing response. The OTS coating of fibre surface was engineered *via* incubation with fixed fluoro-LPS on getting rid of excess LPS. Real time probe efficacy was ascertained from an improved RI sensitivity whereby a glass flow cell having OTS functionalized UFOPs was dipped in samples with varied LPS amounts. Inspection revealed an LPS RI of ~1.5 contrary to 1.45 for bulk OTS solution, due to an additional LPS layer *via* displacing water (RI = 1.33). The LOD with OTS free UFOP was 0.1 μg•mol^{-1}, assuming 10 kDa as LPS molecular weight.

Screening of PMB bound Au NPs at 525 nm revealed an enhanced absorbance, varying exponentially with LPS amount with 1 ng•mL^{-1} as least screened LPS extent; two orders higher than direct assay

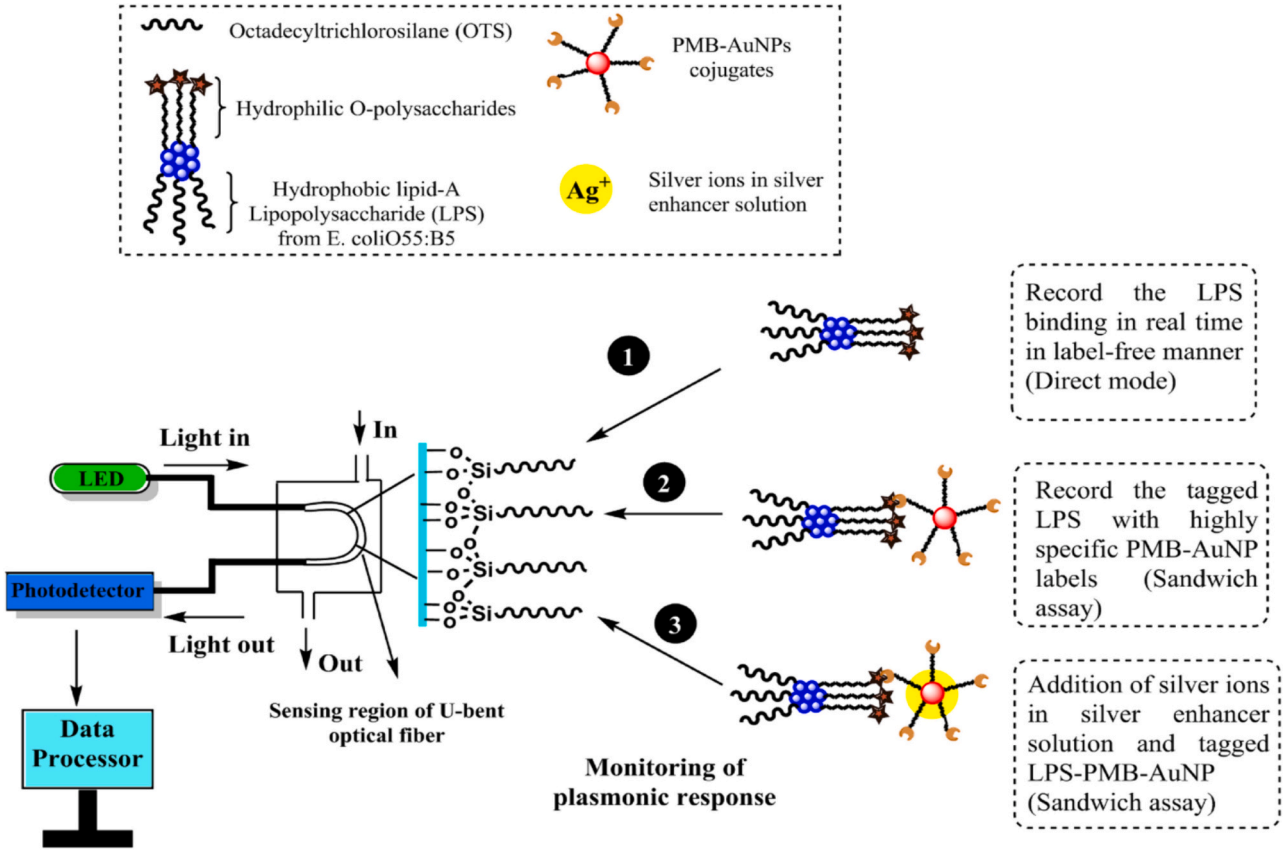

Fig. 12. Fabrication steps forU shaped bent fibre optic probedevelopment and its characterization for sensing response, for the 2018 study of *Zhang and colleagues* [111].

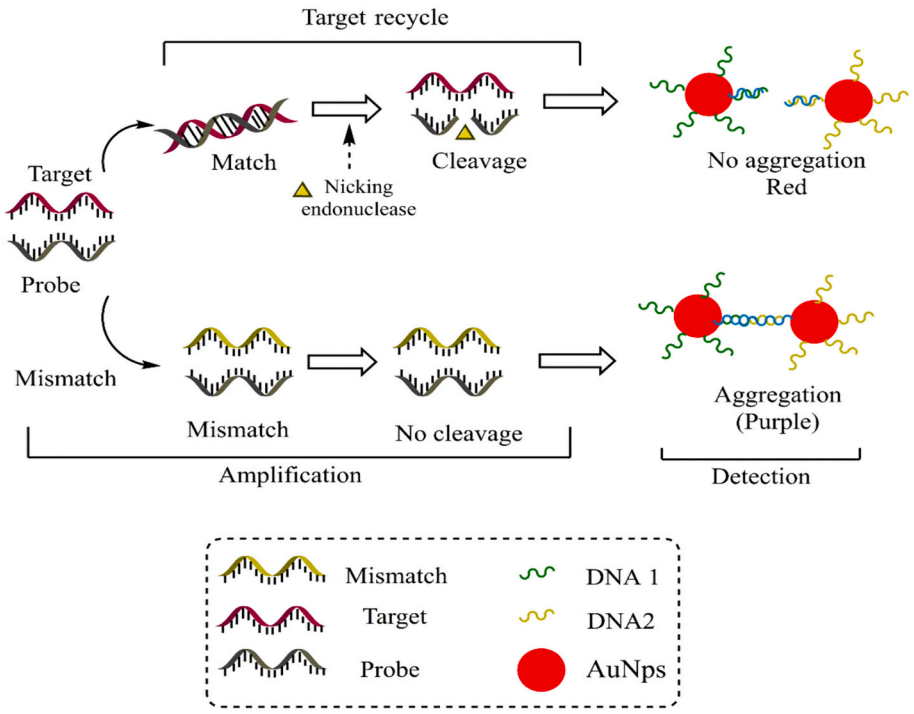

Fig. 13. Optimization of probe design, in terms of amplification and detection procedures for DNA nanoparticles mediated zebra mussel DNA identification in contaminated water samples [116].

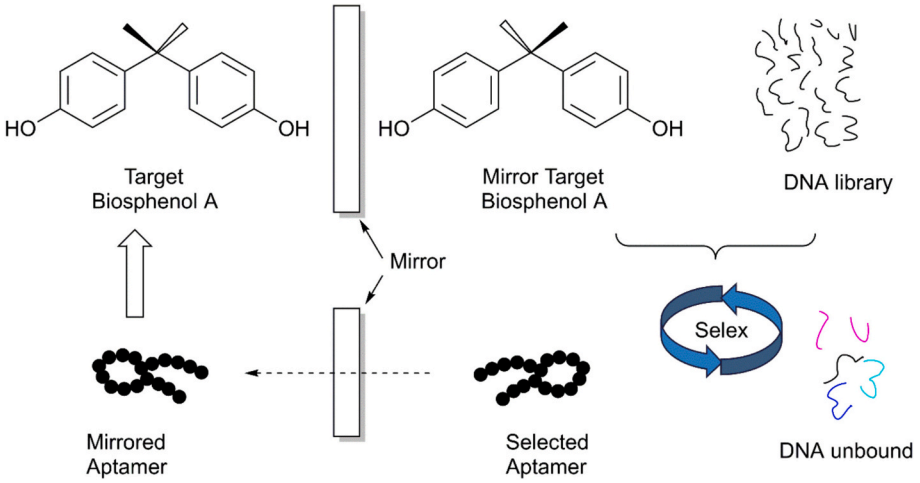

Fig. 14. Optimization of probe design for D-oligonucleotide enantiomers mediated Bisphenol A detection in contaminated water samples [119].

[112,113]. Linear detection within (0.1–100) ng•mL^{-1} with 0.97 correlation coefficient, supported the SEM observations. Specificity inspection for threonine, tyrosine, lactic acid, human immunoglobulin (IgG), normal saline and dextrose normal saline revealed (10−100) folds higher LPS extents. The response was monitored *via* incubation in 100 ng•mL^{-1} LPS-interferers and PMB-Au NPs, revealing least LPS contamination for human IgG with none signal being >15% without interferers. Sensitivity enhancement *via* catalytically assisted Ag deposition on Au NPs, facilitated prompt Ag^{+} reduction and subsequent nucleation [114]. Upon 3 min Ag enriching, unfolded probes exhibited a dose dependent signal with 36 fold higher sensitivity, 0.998 correlation coefficient and a (0.1–100) ng•mL^{-1} linear response. The LOD was 0.4 ng•mL^{-1}, better than sandwich assay regime. The Ag enhancement revealed a large red shift on Ag NPs deposition over the fibre surface

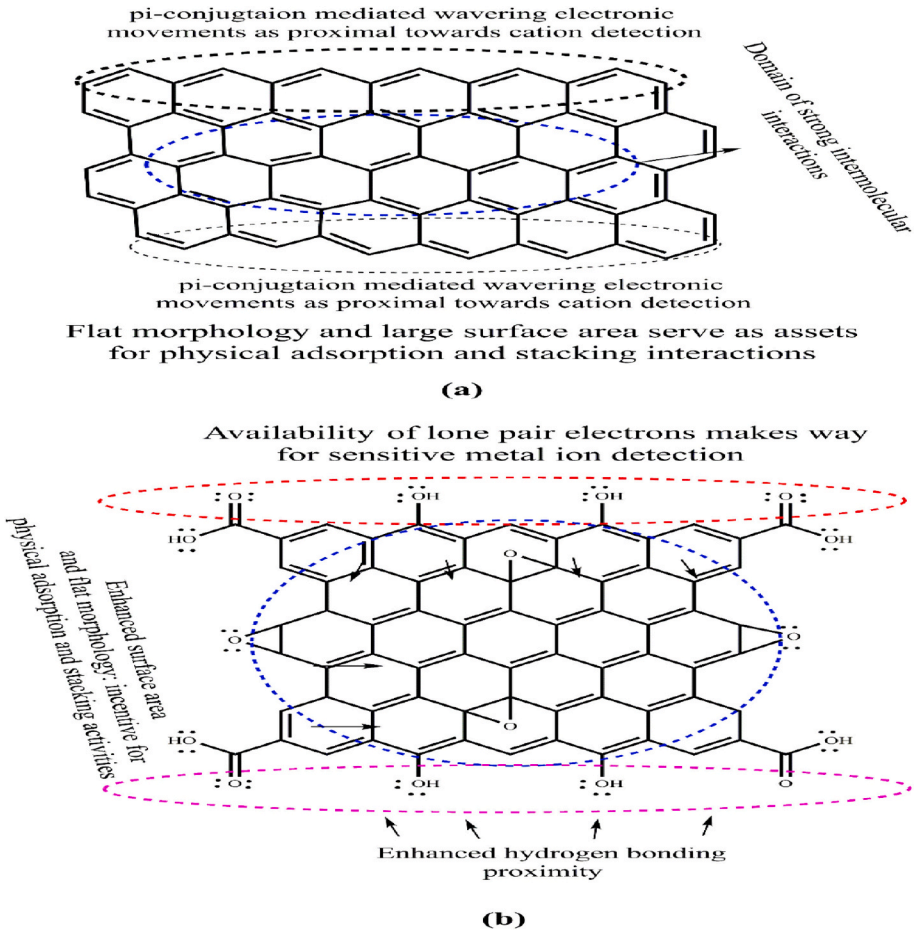

Fig. 15. Schematic representation of (a) sp^2 hybridized pure carbon hexagonal lattice, and (b) representative chemical structure of graphene oxide. While hexagonal lattice depicts the large surface area of graphene the formation of graphene oxide is attributed towards enhanced interactive functionalities *via* conjugated O and –OH functionalities. Varying oxygen contents in graphene oxide formed from graphene are the basis of multiple applications.

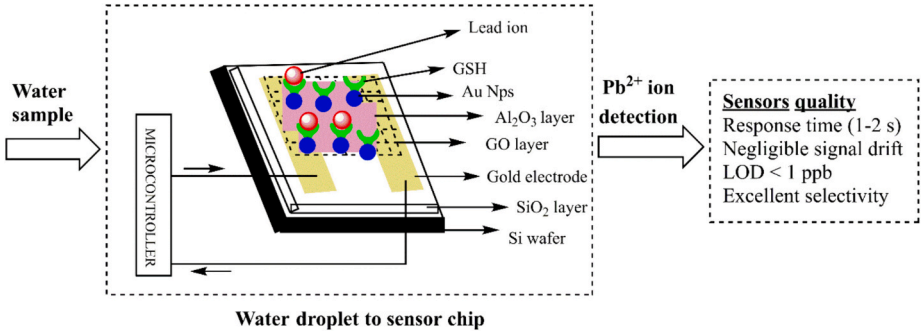

Fig. 16. Pictorial depiction ofsensor chip describing the functional biosensing mode for the 2017 study by *Maity and colleagues* [127].

[115]. Fig. 11b depicts the PMB structure, wherein O, -OH and $–NH_2$ groups manifest a hydrophilic sensitivity. Closer O and $–NH_2$ placements besides –NH, =O, -OH,$–NH_2$ functionalities infer a sensitivity for intra and inter molecular HB. A weaker hydrophobicity with only one AC attributed the probe-analyte interactions a stronger hydrophilic sensitivity.

Next in line is a 2021 effort, wherein target DNA amplification mediated signal enhancement was validated *via* dual mode colorimetric naked eye and smartphone screening, for screening zebra mussel DNA. Of note, zebra mussel is an invasive, fingernail sized mollusk native to Eurasian freshwaters, named so due to zig-zagged shell stripes. Analyte DNA amplification was accomplished *via* nicking endonuclease cleavage of probe-complimentary target hybridization subsequent to which, modified probe interacts with DNA functionalized Au NPs. Fig. 13 depicts a target DNA amplification and detection, improving the naked eye sensitivity by 12 folds for ~8 nM LOD in controlled conditions and 22.5 nM in complex environment. The assay discriminated zebra mussel DNA sequences besides 130 fold improved sensitivity *via* smart-phone monitored environmental samples. The 0.17 nM LOD was highly relevant to gauge aggregation with reduced naked eye subjectivity [116]. Subsequent study using biomolecules functionalized Au NPs for water quality screening used D-oligonucleotide enantiomers for ascertaining bisphenol A (BPA) contamination. Of note, BPA is a prominent plastic monomer widely reported for its endocrine disruptive actions [117,118]. The study exploited aptamer binding ability of D-oligonucleotides enantiomers *via* Biolayer interferometry alongside screening biological stability on nucleases exposure. Fig. 14 depicts the optimized probe configuration as label free Au NPs colorimetric assay for BPA detection with 0.057 ng•mL^{-1} LOD over (100 pg•mL^{-1}-10 mg•mL^{-1}) range [119]. Another 2022 effort from *Ye and colleagues* [120] demonstrated multiplex sensors with specific locus centred aptamer functionalized Au NRs facilitated Pb^{+2} and Hg^{+2} detection. The detection of heavy metals (Pb and Hg) was optimized *via* distinct responses of individual Au NRs with characteristic spectra shifts in the scattering spectrum. Inspection of bound Pb and Hg using a spectral imaging dark field microscope ascertained the response of manifold single plasmonic nanosensors with high time resolution and precision. The LOD for the assay was determined *via* monitoring concentration specific response of position specific nanosensors for Hg^{+2} and Pb^{+2} containing mixtures. Inspection revealed 5 nM (Pb^{+2}) and 1 nM (Hg^{+2}) sensitivities, exhibiting the feasibility to screen other heavy metal ions (alike periodic table groups).

4.4. Gold nanoparticles anchored graphene and reduced graphene assemblies

Large SA and functionalization diversity of graphene and its derivatives are the reasons for their remarkable applications in catalysis, energy storage and conversion. Structural distinctions of graphene include a single, thin layer of tightly packed pure carbon atoms as hexagonal honeycomb lattice with sp^2 hybridization and a 0.142 nm C—C bond length (Fig. 15a). With a thickness of ~one atom and (100−300) times higher strength than steel, graphene oxide (GO) is the most used graphene derivative, prepared *via* graphite oxidation (Fig. 15b). Multiple applications of GO include use in electrodes, solar cells, polymer filler for improved tensile strength, elasticity, conductivity *etc.* [121,122]. The studies using graphene/GO-Au NPs as probes for screening water quality are as discussed ahead.

First major post 2015 study herein, examined NO_3^- *via* absorption spectrum, involving Au NPs interaction with $-NH_2$ modified GO ($-NH_2$@GO), avoiding aggregation due to low NO_3^- amount remaining untraced *via* conventional assay. The optimized probe configuration exhibited a reduced aggregation on NO_3^- and modified GO interaction, screening NO_3^- *via* absorption spectrum, superseding the Au NPs due to anionic impurities. Optimization involved no pretreatment, screening 5 nM NO_3^- in DW, much lower than 161 μM (absorption spectroscopy) [123]. The Au NPs used herein were prepared *via* citrate reduction and optimized *via* 10 min, 8000 rpm centrifugation of their 4 mL quantity on aqueous washing and subsequent dispersion in 0.2 mL H_2O. Real screening was done *via* deliberate NO_3^- contamination on 10 min centrifugation of river water (pH = 7) at 10,000 rpm. Finally, 20 μL, 1 mg•mL^{-1} $-NH_2$@GO was mixed with sample (1:1) and incubated for 1 h at RT, before examining its UV–visible absorption. A decisive step in probe optimization involved ethylenediamine (EDA) modification of GO sheets, prior to $–NH_2$ functionalization. The $-NH_2$@GO mixing with Au NPs induced their aggregation *via* electrostatic interactions, nullified *via* NO_3^- π-aromatic cloud interception of $-NH_2$@GO [124]. Detection sensitivity (ΔR) was monitored *via* subtracting $R_{nitrate}$ to R_{blank} ratios, where $R_{nitrate}$ was 620 to 520 nm absorbance ratio of NO_3^- contaminated samples in UV–visible spectra while R_{blank} was similar extent for blank samples. A high ΔR inferred a NO_3^- contamination with a higher sensitivity, where (1.51–4.53) μg•mL^{-1} increment enhanced ΔR. Since 6.03 μg•mL^{-1} GO decreased the ΔR, 4.53 μg•mL^{-1} was chosen as optimum GO. The investigators noted inadequate signal distinctions for blank and NO_3^- contaminated samples due to excessive aggregation. The optimum incubation for detection sensitivity was ascertained as 1 h. Polarity changes inferred $-NH_2$@GO-NO_3^- interactions, with −29.4 mV ζ-potential for GO being enhanced to −18.9 mV for EDA modified GO and yet again decreasing to −26.6 mV on NO_3^- incubation. These surface polarity changes for NO_3^- neutralizations were supported by SEM and TEM inferred Au NPs aggregation for null and 50 mM NO_3^-. Selectivity was ascertained *via* Cl^-, Br^-, I^-, SO_4^{2-} recognition, where only NO_3^- decreased absorption ratios at 620 and 520 nm (Au NPs SPR) [125]. Commercial feasibility was monitored *via* screening NO_3^- contaminated river water, wherein 5 nM was retrieved as LOD, in river and DW [126]. The sensing precision could be further improved using GO derivatives and highly diverse morphologies for Au NPs shapes and sizes (obtained on altered precursor to reducing agent ratios).

Next in line is a 2017 effort, wherein an ultrasensitive pulse-driven capacitance based Pb^{+2} recognition was accomplished *via* self-assembly driven GO monolayer to monitor the contamination of water samples. Intact field effect transistor (FET) comprised thermally reduced

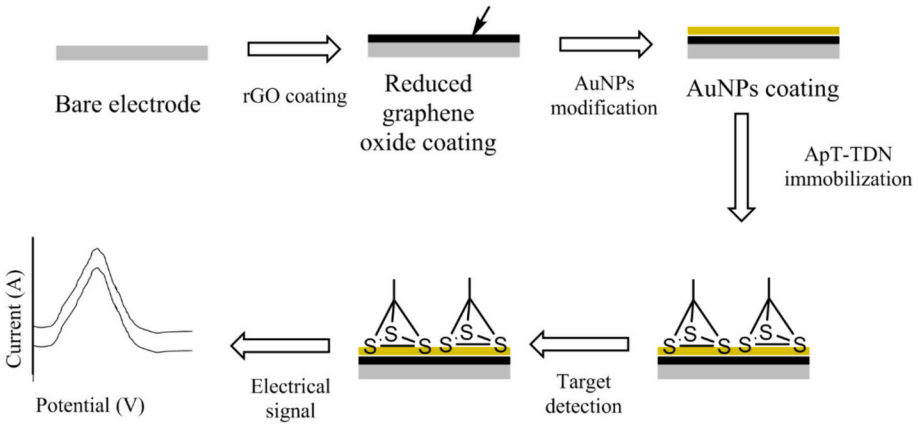

Fig. 17. Optimized probe configuration, comprising Au NPs functionalization on the electrochemically reduced graphene oxide surface and concomitant enrichment by tetrahedral DNA nanostructures for ampicillin detection in aqueous environment [128].

GO channel with a defunct thin Al_2O_3 layer as a top gate combined with sputtered Au NPs conjugated glutathione (GSH) as probe. Fig. 16 summarizes the sensor chip configuration, working module and electronic properties for the probe. For real application, a miniaturized Arduino-based microcontroller was programmed to generate pulses, capacitance signal reading and continuous data recording. The Pb^{+2} probe-specificity was ascertained *via* its insignificant responses for Zn^{+2}, Mg^{+2}, Hg^{+2}, Cd^{+2}, Fe^{+3}, Na^{+} and Ag^{+}. Sensitivity was monitored *via* monitoring real time capacitance transient for Hg^{+2} (5–100 ppb) with Pb^{+2}, revealing an insignificant relative capacitance change for Hg^{+2} solution. Commercial feasibility was adjudged *via* water samples from the city of Flint, fresh tap water from Milwaukee, Lake Michigan and river Mailwaukee, revealing agreements with ICP analysis for Flint water, having 2.38 ppb Pb^{+2} than <0.8 ppb for others. The 180 and 30% capacitance transient responses for Flint water and Milwaukee tap water enabled a (0.4–2.38) ppb Pb^{+2} screening in Flint water. The assay time for background stabilization subsequent to Pb^{+2} monitoring was ascertained as 10 s, was much lower than FET resistance (in min) and inductive/optical plasma methods (in hours). Approximate linear range (5–20) ppb estimation for ~15 ppb extent projects probe suitability for drinking water [127]. Intriguingly, functionalization with doped graphene could improvise the accuracy *via* reduced interception time. The optimized configuration (rGO passivated by thin Al_2O_3 as top gate with GSH functionalized sputtered Au NPs) could be engineered for other impurities too. Besides, portable configuration could be employed in remote locations and moderate economies.

Latest attempt in rGO-Au NPs screened water quality is a 2022 study whereby, aptamer mediated electrochemical sensing was optimized *via* surface engineering and DNA nanotechnology to monitor ampicillin contamination in animal products. The working electrode was modified in SPCE *via* electrochemically rGO and Au NPs enhanced electrochemical conductivity (Fig. 17). Subsequent surface engineering *via* self-assembled tetrahedral DNA nanostructures (TDN) improved the detection sensitivity, *via* aptamer nano-spacing immobilized over electrode surface. These aptamers were put in solution for target binding, and accessed *via* differential pulse voltammetry for bound ampicillin extents. Analysis revealed a (10 pM-1 mM) detection in <30 min with 1 pM LOD, ~100 folds higher than without TDN functionality. Feasibility monitoring revealed a reusable tendency on DW rinsing besides 15 day storage stability and reproducibility [128].

4.5. Miscellaneous platform configurations of Au nanoparticles as water sensors

An integrated approach using microfluidics and porosity modulated papers as sensing platforms (microfluidic paper based provisions, μPADs) *vis-à-vis* laser printing (LP) devices feasibility for pesticide screening in aqueous conditions. Optimized probe configuration was accomplished *via* studies with varied paper platform porosities, textures and channel thickness. The Au NPs for the probe were prepared using citrate reduction, ensured *via* terminal colour change to blue. The as prepared NPs were thoroughly screened for their nanoscale traits, using DLS, UV–Vis spectroscopy and SEM. Optimized LP-μPAD configuration was prepared using Adobe illustrator software (V2019), wherein a laser printer was employed to print a hydrophobic barrier over the filter paper having a highest printing ability (600 DPI). Printed filter papers were uniformly heated in an incubator at 170 °C till 30 min (forming requisite hydrophobic barrier) to ensure optimum paper impregnation with toner ink. The 2023 effort from Turkey involved a thorough probe characterization to screen the titre of atrazine (a chlorinated triazine systemic herbicide used to selectively control the annual grasses and broadleaf weeds prior to their emergence) in water *via* colorimetric assessments using a smart-phone assisted imaging. Analysis revealed an LOD of 10.9 μM with high repeatability and reproducibility. Thereby, the probe configuration in this study conceptualized a successful integration of laser assisted viewing across the microfluidic, capillary flow assisted paper channels for specific detection of pesticides. Interference studies revealed the pesticide screening as unaffected by added NaCl quantities and varied pH levels. On the whole, the study presented LP assisted capillary flow monitoring as effective and low-cost remedy for accessible water quality monitoring [129].

5. Summary and future directions

We have presented a comprehensive account of Au NPs sensing distinctions (shape-size modulated structure-function diversity) alongwith the discussion of prominent research attempts using their diversified regimens for screening the contamination of water resources. The reason for unceremonious interest in Au NPs as sensing moieties for validating the upright quality of water resources is the remarkable stability of Au which assists in their robust functionalization. Besides the steadfastness of manifold reproducible and nature friendly preparation methods (largely bottom-up) with a well-understood mechanism and physical indications are the additional impetus. The first mechanism of Au NPs use in biosensing relies on their monodispersed or aggregated state variations in SPR. Second workable strategy involves the coating of electrodes with Au nanothin films (due to electrically conductive nature of Au). Third strategy towards Au NPs use as water quality assessment agents involves their functionalization with biomolecules such as antibodies, engineered DNA or RNA fragments, proteins, carbohydrate derivatives and others. This configuration of Au NPs could be used for *in vivo* screening owing to a compatible functioning of the probe. Fourth

Table 3
Summary of post 2000 studies with a brief description of probe configurations and major findings, complete discussion of these attempts features in the text.

Sensed stimulus	Sensing configuration of Au NPs	Response characteristics (linear range, LOD and sensitivity)	Reference
Singular or combinatorial existence driven SPR changes			
Aflatoxin B1-MRS	Dumbbell similar Au-Fe_3O_4 NPs as magnetic nanoprobes	• Au NPs as core facilitated the growth of Ag shell and gather Au-Fe_3O_4 NPs, modulating transverse relaxation time of neighbouring water molecules • Ag(shell)-Au-Fe_3O_4 core-shell NPs as probe were generated by H_2O_2 • On horseradish peroxidase degradation, H_2O_2 reduces Ag^{+} to Ag^{0}, accumulating dispersed Au-Fe_3O_4 as Ag@Au-Fe_3O_4 NPs • With 3.81 pg•mL^{-1} sensitivity, the Ag@Au-Fe_3O_4 NPs as nanoprobes • 21 and 9 folds better efficacy than ELISA and HPLC • Consistency with HPLC for real samples inferred accuracy for optimized configuration.	[97]
Escherichia coli contamination	Au@MnO_2 NPs in core-shell morphology having MnO_2 as shell	• LOD: 15 CFU•mL^{-1} • Dynamic range: (100–2900) CFU•mL^{-1} • Ultrasensitive and low cost *E. coli* screening in river water	[98]
Hg^{+2}	Au@Ag core-shell NPs as SERS substrates while rhodamine 6G (R6G) as a Hg^{+2} signaling probe	• Hg^{+2} screening accomplished *via* quenching of R6G strong SERS signal on interaction with Au@Ag NPs, slowly replacing Ag^{+} by bound Hg^{+2} • Blue shift in UV–Vis SPR peak of Ag shell of Au@Ag NPs, reducing Hg^{+2} to Hg^{0} on Ag shell surface of Au@Ag NPs, on Hg^{+2}-citrate ion of Au@Ag NPs complex formation • 0.9745 and 0.9773 as correlation coefficients within (10^{2}–10^{-3}) µg•g^{-1} • (88.45–94.73)% recovery and (3.28–5.76)% as coefficient of variations	[99]
Electrochemical Configurations			
Pb^{+2}	Au NPs-Ppy-$Ti_3C_2T_x$ nanocomposite prepared *via* layered self assembly PPy is an organic polymer retrieved *via* oxidative polymerization of pyrrole	• XPS and XRD inspections revealed $Ti_3C_2T_x$ significance in PPy formation, alignment and Au NPs growth • Au NPs facilitated covalent linkage, *via* Au—S functionality • Response analysis inferred a 5•10^{-14}-1•10^{-8} M linear working range with 1•10^{-14} M LOD • Good selectivity and sensitivity for Pb^{+2} in Nong Fu spring and tap water • *E. coli* identification was accomplished *via* square-wave, differential pulse and cyclic voltammetry	[105]
Escherichia coli screening in pharmaceuticals or certain real samples	• Multi-walled CNTs-Au NPs-*E. coli* polyclonal Ab-BSA optimized at pH = 7 using PBS buffer • Acetaminophen was added for *E. coli* detection *via* conductivity and current variations	• Square-wave voltammetry revealed 3.02 CFU•mL^{-1} as LOD 3 min with adequate sensitivity, repeatability and reproducibility • Could be explored for drug safety, quality control, clinical diagnostics and environmental assessment	[106]
Au NPs functionalized with compatible biomolecules			
Zebra mussel DNA (an invasive, fingernail sized mollusk)	Nicking endonuclease assisted Au NPs signal amplification	• 12 fold higher naked eye sensitivity • LOD: ~8 nM in controlled and 22.5 nM in complex environment • Smartphone improved sensitivity by 130 folds with 0.17 nM LOD, • Probing aggregation tracking with increased accuracy and reduced naked eye subjectivity	[116]
Bisphenol A (widely reported for its endocrine disruptive activities)	First ever use of nuclease resistant spiegelmer in a label-free Au NP based colorimetric assay	• Aptamer-target interactions supported by chemically made spiegelmers were screened using biolayer interferometry	[119]

(*continued on next page*)

Table 3 (*continued*)

Sensed stimulus	Sensing configuration of Au NPs	Response characteristics (linear range, LOD and sensitivity)	Reference
Pb^{2+} and Hg^{2+}	Multiplexed nanosensors having locus fixation aptamer functionalized Au NRs	• Stabilities in multiple biofluids was examined *via* exposure to nucleases • 0.057 ng•mL^{-1} LOD over (100 pg•mL^{-1} to 10 mg•mL^{-1}) range. • Highly sensitive and selective efficacy, non-biodegradable platform for sensitive bisphenol A detection • Home-built spectral imaging dark-field microscope screened thousands of single plasmonic nanosensors • Explicit Au NRs responded to Pb^{+2}, Hg^{+2} *via* discrete SPR alterations • LOD: 5 nM for Pb^{2+} and 1 nM for Hg^{2+}, exhibiting suitability for other heavy metal ions too	[120]
Au NPs functionalized Graphene oxide or its functionalized derivatives			
Antibiotic ampicillin	Electrochemically reduced graphene oxide-Au NPs surface coated by self-assembled tetrahedral DNA nanostructures	• (10 pM-1 mM) detection in <30 min with 1 pM LOD • ~100 fold better than without TDN. • Reusable platform on rinsing with deionized water besides 15 day storage stability and reproducibility	[128]
Integrated Configurations (Not matching any of the above)			
Atrazine (a pesticide)	Dual chromatic laser-printed microfluidic paper-based analytical device (μPAD)	• LP assisted capillary flow as effective and low-cost remedy for accessible water quality monitoring • Optimized LP-μPAD was prepared using Adobe illustrator, wherein a LP aided imprint of a hydrophobic barrier over the 600 DPI ability filter paper • Atrazine titre was screened using 170 °C dried filter papers *via* colorimetric assessments and a smart-phone assisted imaging • LOD of 10.9 μM with high repeatability and reproducibility	[129]

Abbreviations: SPR: surface plasmon resonance, MRS: magnetic relaxation switching, MOF: metal organic framework, IgG: immunoglobulin G, NPs: nanoparticles, NRs: nanorods, LOD: Limit of Detection, MDIA: 10-mercaptodecyl-1-iminodiacetic acid, LPS: lipopolysaccharide, NPs: nanoparticles, PPy: polypyrrole, FAM: carboxyfluoroscein, GO: Graphene oxide, GSH: glutathione, ppb: parts per billion, LP: laser printer, rGO: reduced graphene oxide.

configuration of Au NPs monitored water quality involves their functionalization over the surface-active graphene oxide and its related configurations. Functionalization holds the backbone aspects of Au NPs use in water quality monitoring and could be done in covalent/non-covalent mode to engineer the interaction potentials. Table 3 summarizes the post 2020 attempts for the discussed Au NPs configurations where the LOD differences convey the precision sensitivity of miniaturized dimensions. Distinct responses are the typical outcomes of characteristic size-shape modulations wherein quantum effects are exhibited at ease with larger SA. Future insights for similar applications of Au NPs could be consolidated *via* ascertaining a reproducible performance of their composite configurations alongwith improving their specific response. Docking simulations for integrated prevalence and optimized combinations with Au NPs could help predict their stability and a transition driven energetic excitations and de-excitations. Enhanced precision of characterization techniques is a crucial aspect of reliance for such diversified applications of Au NPs. Collaborative participation of chemists with material scientists and electronics expert could strengthen the Au NPs accuracy further with the integration of micro and nano electromechanical systems (NEMS and MEMS) could still fasten the read out mechanisms of analyte-probe interactions. Micromachining and surface engineering of NMs alongwith predictive *in situ* tools consolidate the constitutional energy levels for infinitesimal responses.

6. Conclusions

The native state high stability of Au NPs encompassing their manifold functionalization, consolidates their dynamic shape-size modulated PCPs. Although singular or combined use of Au NPs remains the most understood mechanism working *via* reversible aggregation, functionalization has recently turned the attention to biomolecules coupled Au NPs assay. Despite sophisticated characterization *via* CV and EIS, better probe performance could be accomplished subject to computational assessment of combinatorial stoichiometry stability. As lifestyle changes and industrialization loom high, there is a need for high precision assisted sensing tools wherein Au NPs as the emerging frontrunners. Contaminations like antibiotics, pesticides and microbial colonies are prominent interferers in edible texture of water resources at large. Perhaps the scenario urgently needs co-operation between engineers and bio-scientists for diligent detection efficacy and time-lapse of interactions. Cautions must be exercised for a characterization specific size and functionalization abilities. These cautions must warn with results of earlier findings so that sustainability aspect is not tampered with. Likewise a rigorous tract of known response time (size-shape artefacts, reducing and capping agents for making Au NPs) must be adequately referred and update so that necessary cautions and resource conservation could be strengthened in future attempts.

Declaration of competing interest

The authors declare that they have no known competing financial interests or personal relationships that could have appeared to influence the work reported in this paper.

Data availability

Data will be made available on request.

References

[1] S. Madhav, A. Ahamad, A.K. Singh, J. Kushawaha, J.S. Chauhan, S. Sharma, P. Singh, Water pollutants: Sources and impact on the environment and human health, in: Sensors in Water Pollutants Monitoring: Role of Material, Springer Publications, 2019, p. 43, https://doi.org/10.1007/978-981-15-0671-0_4.

[2] Y. Orooji, H. Sohrabi, N. Hemmat, F. Oroojalian, B. Baradaran, A. Mokhtarzadeh, M. Mohaghegh, H. Karimi-Maleh, An overview on SARS-CoV-2 (COVID-19) and other human coronaviruses and their detection capability via amplification assay, chemical sensing, biosensing, immunosensing, and clinical assays, Nano-Micro Lett. 13 (2021) 1, https://doi.org/10.1007/s40820-020-00533-y.

[3] H. Sohrabi, M.R. Majidi, F. Nami, K. Asadpour-Zeynali, A. Khataee, A. Mokhtarzadeh, A novel engineered label-free Zn-based MOF/CMC/AuNPs electrochemical genosensor for highly sensitive determination of *Haemophilus Influenzae* in human plasma samples, Microchim. Acta 188 (2021) 100, https://doi.org/10.1007/s00604-021-04757-6.

[4] N. Xiao, Using Functionalized Nanoparticles as Sensors for Rapid Monitoring of Drinking Water Quality, Iowa State University, 2010. Retrieved from https://lib.dr.iastate.edu/etd.

[5] F. Bullough, C. Fenech, H. Bridle, Advances in water quality monitoring of inorganics: current trends, J. Water Resource & Prot. 5 (2013) (2013) 40–48, https://doi.org/10.4236/jwarp.2013.54A007.

[6] Y. Du, X. Xu, Q. Liu, L. Bai, K. Hang, D. Wang, Identification of organic pollutants with potential ecological and health risks in aquatic environments: Progress and challenges, Sci. Total Environ. 806 (2022) 150691, https://doi.org/10.1016/j.scitotenv.2021.150691.

[7] M. Patel, R. Kumar, K. Kishor, T. Mlsna, C.U. Pittman Jr., D. Mohan, Pharmaceuticals of emerging concern in aquatic systems: chemistry, occurrence, effects, and removal methods, Chem. Rev. 119 (2019) 3510–3673, https://doi.org/10.1021/acs.chemrev.8b00299.

[8] P. Malik, R.K. Ameta, in: Ashok Rathoure (Ed.), A Green and Sustainable Tool for Physicochemical Analysis of Liquid Solutions in Survismeter in Zero Waste: Management Practices for Environmental Sustainability, First Edtn, Taylor & Francis Group- CRC Press, Florida, USA, 2019 (978–0–367-18039-3.

[9] P. Malik, T.K. Mukherjee, M. Singh, Biomedical nanotoxicology and concerns with environment: a prospective approach for merger with green chemistry enabled physicochemical characterization, J. Microb. & Biochem. Technol. S9 (2014) 001, https://doi.org/10.4172/1948-5948.S9-001.

[10] A. Rompre, P. Servais, J. Baudart, M.R. De-Roubin, P. Laurent, Detection and enumeration of coliforms in drinking water: current methods and emerging approaches, J. Microbiol. Methods 49 (2002) 31–54, https://doi.org/10.1016/S0167-7012(01)00351-7.

[11] T. Dhewa, Biosensor for environmental monitoring: an update, Octa J. Env. Res. ISSN: 2321-3655 3 (2015) 212–218.

[12] P. Malik, V. Katyal, V. Malik, A. Asatkar, G.K. Inwati, T.K. Mukherjee, Nanobiosensors: concepts and variations, ISRN Nanomater. (2013) 327435, https://doi.org/10.1155/2013/327435.

[13] P. Malik, R. Gupta, V. Malik, R.K. Ameta, Emerging nanomaterials for improved biosensing, Meas: Sens. 16 (2021) 10050, https://doi.org/10.1016/j.measen.2021.100050.

[14] P. Malik, R. Shankar, V. Malik, N.K. Sharma, T.K. Mukherjee, Green chemistry based benign routes for nanoparticle synthesis, J. Nanopart. (2014) 302429, https://doi.org/10.1155/2014/302429.

[15] P. Malik, T.K. Mukherjee, Recent Progress in gold and silver nanoparticles biomedical attributes towards lung and breast cancer treatment, Int. J. Pharm. 553 (2018) 483–509, https://doi.org/10.1016/j.ijpharm.2018.10.048.

[16] P. Malik, R.K. Ameta, in: Dr. Sudip Basu (Ed.), Recent Progress in au Nanoparticle Treatment of Lung Cancers in Biomedical Engineering and its Applications in Healthcare, Springer Nature Publications, 2020, 978–981–13-3705-5.

[17] P. Malik, G.K. Inwati, R. Gupta, T.K. Mukherjee, in: Suban Sahoo, M. Reza Hormozi-Nezhad (Eds.), Recent progress in gold and silver nanoparticle mediated drug delivery to breast cancers, in Gold and Silver Nanoparticles, Synthesis and Applications, Elsevier Publications, 2023, pp. 291–328, https://doi.org/10.1016/B978-0-323-99454-5.00012-3.

[18] S. Mourdikoudis, R.M. Pallares, N.T.K. Thanh, Characterization techniques for nanoparticles: comparison and complementarity upon studying nanoparticle properties, Nanoscale 10 (2018) 12871–12934, https://doi.org/10.1039/C8NR02278J.

[19] G. Doria, J. Conde, B. Veigas, L. Giestas, C. Almeida, M. Assunção, J. Rosa, P. V. Baptista, Noble metal nanoparticles for biosensing applications, Sensors 12 (2012) 1657–1687, https://doi.org/10.3390/s120201657.

[20] H.A. Atwater, The promise of plasmonics, Sci. Am. 296 (2007) 56–63. 17479631.

[21] E. Ozbay, Plasmonics: merging photonics and electronics atnanoscale dimensions, Sci 311 (2006) 189–193, https://doi.org/10.1126/science.1114849.

[22] S.A. Maier, H.A. Atwater, Plasmonics: localization and guiding of electromagnetic energy in metal/dielectric structures, Appl. Phys. Lett. 98 (2005) 1–10, https://doi.org/10.1063/1.1951057.

[23] L. Wang, W. Ma, L. Xu, W. Chen, Y. Zhu, C. Xu, N.A. Kotov, Nanoparticle-based environmental sensors, Mater. Sci. Eng. R R70 (2010) 265–274, https://doi.org/10.1016/j.mser.2010.06.012.

[24] C.J. Murphy, Nanocubes and nanoboxes, Sci 298 (2002) 2139–2141, https://doi.org/10.1126/science.1080007.

[25] C.M. Niemeyer, U. Simon, Eur., DNA-based assembly of metal nanoparticles, J. Inorg. Chem. 18 (2005) 3641–3655, https://doi.org/10.1002/ejic.200500425.

[26] K. Kneipp, H. Kneipp, H.G. Bohr, Single-molecule SERS spectroscopy, Appl. Phys. 103 (2006) 261–278, https://doi.org/10.1007/3-540-33567-6_13.

[27] D.A. Oliveira, J.V. Silva, J.M.R. Flauzino, A.C.H. Castro, A.C.R. Moço, M.M.C. N. Soares, J.M. Madurro, A.G. Brito-Madurro, Application of nanomaterials for the electrical and optical detection of the hepatitis B virus, Anal. Biochem. 549 (2018) 157–163, https://doi.org/10.1016/j.ab.2018.03.023.

[28] I. Khalil, N.M. Julkapli, W.A. Yehye, W.J. Bairum, S.J. Bhargava, Graphene-gold nanoparticles hybrid-synthesis, functionalization, and application in a electrochemical and surface-enhanced Raman scattering biosensor, Materials 9 (2016) 406, https://doi.org/10.3390/ma9060406.

[29] C.L. Braun, S.N. Smirnov, Why is water blue? J. Chem. Educ. 70 (1993) 612–614.

[30] F. Franks, Water: a comprehensive treatise. The physics and physical chemistry of water, P. P. 1 (1972).

[31] A. Ben-Naim, Statistical Thermodynamics for Chemists and Biochemists, Springer, 1992, pp. 459–559.

[32] E. Brini, C.J. Fennell, M. Fernandez-Serra, B. Hirbar-Lee, M. Luksic, K.L. Dill, How water's properties are encoded in its molecular structure and energies, Chem. Rev. 117 (2017) 12385–12414, https://doi.org/10.1021/acs.chemrev.7b00259.

[33] R.K. Mahajan, T.P.S. Walia, B.S. Lark, Sumanjit, Analysis of physical and chemical parameters of bottled drinking water, Int. J. Environ. Health Res. (2007) 89–98, https://doi.org/10.1080/09603120500538184.

[34] D.L. Johnson, S.H. Ambrose, T.J. Bassett, M.L. Bowen, D.E. Crummey, J. S. Isaacson, D.N. Johnson, P. Lamb, M. Saul, A.E. Winter-Nelson, Meanings of environmental terms, J. Environ. Qual. 26 (1997) 581–589.

[35] A. Jordan, Jordanian standards for drinking water, Ministry of Water and Irrigation, World Health Organization (1996) Guidelines for drinking water quality 2nd edition, 2, 2001. Geneva.

[36] WHO Guidelines for Drinking Water Quality, 1996.

[37] R. Bhateria, D. Jain, Water quality assessment of lake water: a review, Sustain. Water Resour. Manag. 1 (2016) 161–173, https://doi.org/10.1007/s40899-015-0014-7.

[38] N. Diersing, Water Quality: Frequently Asked Questions, Florida Brook Keys National Marine Sanctuary, Key West, FL, 2009 https://nmsfloridakeys.blob.core.windows.net/floridakeysprod/media/archive/scisummaries/wqfaq.pdf.

[39] Z.L. He, X.E. Yang, P.J. Stoffella, Trace elements in agroecosystems and impacts on the environment, J. Trace Elem. Med. Biol. 19 (2005) 125–140, https://doi.org/10.1016/j.jtemb.2005.02.010.

[40] M. Kapahi, S. Sachdeva, Bioremediation options for heavy metal pollution, J Health Pollut. 9 (2019) 191203, https://doi.org/10.5696/2156-9614-9.24.191203.

[41] Agency for Toxic Substances and Disease Registry (ATSDR) Case Studies in Environmental Medicine - Lead Toxicity, Atlanta: Public Health Service, U.S. Department of Health and Human Services, Weblink: https://www.atsdr.cdc.gov/csem/lead/docs/lead.pdf, 1992.

[42] C.G. Yedjou, P.B. Tchounwou, Oxidative stress in human leukemia cells (HL-60), human liver carcinoma cells (HepG2) and human Jerkat-T cells exposed to arsenic trioxide, Metal Ions Biol Med. 9 (2006) 298–303. 26435679.

[43] A. Patlolla, C. Barnes, C. Yedjou, V. Velma, P.B. Tchounwou, Oxidative stress, DNA damage and antioxidant enzyme activity induced by hexavalent chromium in Sprague Dawley rats, Environ. Toxicol. 24 (2009) 66–73, https://doi.org/10.1002/tox.20395.

[44] J. Dalmieda, P. Kruse, Metal cation detection in drinking water, Sensors (Basel). 19 (2019) 5134, https://doi.org/10.3390/s19235134.

[45] P.V. Khadikar, S. Karmarkar, S. Singh, A. Shrivastava, Use of the PI index in predicting toxicity of nitrobenzene derivatives, Bioorg. Med. Chem. 10 (2002) 3163–3170, https://doi.org/10.1016/S0968-0896(02)00211-0.

[46] S.S.R. Dasary, A.K. Singh, D. Senapati, H. Yu, P.C. Ray, Gold nanoparticle based label-free SERS probe for ultrasensitive and selective detection of trinitrotoluene, J. Am. Chem. Soc. 131 (2009) 13806–13812, https://doi.org/10.1021/ja905134d.

[47] I.A. Saleh, N. Zouari, M.A. Al-Ghouti, Removal of pesticides from water and wastewater: chemical, physical and biological treatment approaches, Environ. Technol. Innov. 19 (2020) 101026, https://doi.org/10.1016/j.eti.2020.101026.

[48] J. Wolfram, S. Stehle, S. Bub, L.L. Petschick, R. Schulz, Insecticide risk in US surface waters: drivers and spatiotemporal modeling, Environ. Sci. Technol. 53 (2019) 12071–12080, https://doi.org/10.1021/acs.est.9b04285.

[49] R. Raanan, K.G. Harley, J.R. Balmes, A. Bradman, M. Lipsett, B. Eskenazi, Early-life exposure to organophosphate pesticides and pediatric respiratory symptoms in the CHAMACOS cohort, Environ. Health Perspect. 123 (2015) 179–185, https://doi.org/10.1289/ehp.1408235.

[50] J.P. Meneely, J. Hajšlová, R. Krska, C.T. Elliott, Assessing the combined toxicity of the natural toxins, aflatoxin B1, fumonisin B1 and microcystin-LR by high content analysis, Food Chem. Toxicol. 121 (2018) 527–540, https://doi.org/10.1016/j.fct.2018.09.052.

[51] M. Elliott, Biological pollutants and biological pollution-an increasing cause for concern, Mar. Pollut. Bull. 46 (2003) 275–280, https://doi.org/10.1016/S0025-326X(02)00423-X.

[52] J.Y. Lim, J.W. Yoon, C.J. Hovde, A brief overview of *Escherichia coli* O157:H7 and its plasmid O157, J. Microbiol. Biotechnol. 20 (2010) 5–14. PMC3645889.

[53] E. Anderson, L.R. Ward, M.J. de Saxe, J.D.H. De Sa, Bacteriophage-typing designations of *Salmonella typhimurium*, Epidemiol. Infect. 78 (1977) 297–300, https://doi.org/10.1017/S0022172400056187.

[54] J. Wang, J. Wu, Occurrence and potential risks of harmful algal blooms in the East China Sea, Sci. Total Environ. 407 (2009) 4012–4021, https://doi.org/10.1016/j.scitotenv.2009.02.040.

[55] J. Sandnes, T. Ringstad, D. Wenner, P. Heyerdahl, T. K€allqvist, H. Gislerød, Real-time monitoring and automatic density control of large-scale microalgal cultures

using near infrared (NIR) optical density sensors, J. Biotechnol. 122 (2006) 209–215, https://doi.org/10.1016/j.jbiotec.2005.08.034.
[56] G.P. Vieira, S.R.W. Perdigao, M.F. Fiore, B.F. Reis, Development of a high sensitive automatic setup for screening of microcystins in surface waters by employing a LED-based photometric detector, Sensors Actuators B Chem. 161 (2012) 422–428, https://doi.org/10.1016/j.snb.2011.10.054.
[57] Y.-H. Shin, J.Z. Barnett, E. Song, M.T. Gutierrez-Wing, K.A. Rusch, J.-W. Choi, A portable fluorescent sensor for on-site detection of microalgae, Microelectron. Eng. 144 (2015) 6–11, https://doi.org/10.1016/j.mee.2015.01.005.
[58] L. Wang, W. Ma, L. Xu, W. Chen, Y. Zhu, C. Xu, N.A. Kotov, Nanoparticle-based environmental sensors, Mater. Sci. Eng. R. Rep. 70 (2010) 265–274, https://doi.org/10.1016/j.mser.2010.06.012.
[59] V.K. Yadav, S.H. Khan, P. Malik, A. Thappa, R. Suriyaprabha, R.K. Ravi, N. Choudhary, H. Kalasariya, G. Gnanamoorthy, Microbial synthesis of nanoparticles and their applications for wastewater treatment. In: Microbial Biotechnology: Basic Research and Applications, in: J. Singh, A. Vyas, S. Wang, R. Prasad (Eds.), Environmental and Microbial Biotechnology, Springer, Singapore, 2020, pp. 147–187.
[60] V.K. Yadav, N. Choudhary, S.H. Khan, P. Malik, G.K. Inwati, R. Suriyaprabha, R. K. Ravi, Synthesis and characterisation of nano-biosorbents and their applications for waste water treatment, in: Handbook of Research Developments and Environmental Impacts of Ecological Chemistry, 2020, pp. 252–290.
[61] R. Rani, M. Barnela, P. Malik, T.K. Mukherjee, Nanobiofertilizers: Applications and future prospects, in: R.K. Sindhu, M. Chitkara, I.S. Sandhu (Eds.), Nanotechnology: Principles and Applications, Jenny Stanford Publishing Pte. Ltd, 2021. ISBN (Hardcover): 978–981-4877-43-5.
[62] R. Gupta, P. Malik, Nano-Biotechnological Applications for Crop Improvement, In Handbook of Sustainable Agriculture in the Era of Climate, Springer Nature International (Netherlands), 2020, pp. 615–641.
[63] M. Kah, Nanopesticides and nanofertilizers: emerging contaminants or opportunities for risk mitigation? Front. Chem. 3 (2015) 64, https://doi.org/10.3389/fchem.2015.00064.
[64] P. Malik, M. Singh, R.K. Ameta, Advances in Oxidative Stability Mechanisms of Emulsions, in: Ali Aboudzadeh Md (Ed.), Emulsion-based Encapsulation of Antioxidants, Springer Publications, 2020, pp. 311–337.
[65] D.E. Benson, Reagentless biosensors based on nanoparticles, in: Nanotechnologies for the Life Sciences: Online, 2007, https://doi.org/10.1002/9783527610419.ntls0093.
[66] S. Zeng, K.T. Yong, I. Roy, X.Q. Dinh, A review on functionalized gold nanoparticles for biosensing applications, Plasmonics 6 (2011) 491–506, https://doi.org/10.1007/s11468-011-9228-1.
[67] G.V. Buxton Radiation Chemistry: Principles and Applications; Verlag Chemie Publishers: Weinheim, Germany, 1987, D. Soumya, Critical review of water radiolysis processes, dissociation products, and possible impacts on the local environment: a geochemist's perspective, Aust. J. Chem. 66 (2013) 522–529.
[68] E. Gharibshahi, E. Saion, A. Ashraf, L. Gharibshahi, Size-controlled and optical properties of platinum nanoparticles by gamma radiolytic synthesis, Appl. Radiat. Isot. 130 (2017) 211–217, https://doi.org/10.1016/j.apradiso.2017.09.012.
[69] L.F. de Freitas, G.H. Costa Varca, J.G. dos Santos Batista, A.B. Lugao, An overview of the synthesis of gold nanoparticles using radiation technologies, Nanomat 8 (2018) 939, https://doi.org/10.3390/nano8110939.
[70] T.K. Sau, A.L. Rogach, F. Jaeckel, T.A. Klar, J. Feldmann, Properties and applications of colloidal non-spherical noble metal nanoparticles, Adv. Mater. 22 (2011) 1805–1825, https://doi.org/10.1002/adma.200902557.
[71] A. Kumar, Y. Chisti, U. Chand, Synthesis of metallic nanoparticles using plant extracts, Biotechnol. Adv. 31 (2013) 346–356, https://doi.org/10.1016/j.biotechadv.2013.01.003.
[72] S.S. Dash, B.G. Bag, Synthesis of gold nanoparticles using renewable *Punica granatum* juice and study of its catalytic activity, Appl. Nanosci. 4 (2014) 55–59, https://doi.org/10.1007/s13204-012-0179-4.
[73] C. Jayaseelan, R. Ramkumar, A.A. Rahuman, P. Perumal, Green synthesis of gold nanoparticles using seed aqueous extract of *Abelmoschus esculentus* and its antifungal activity, Ind. Crop. Prod. 45 (2013) 423–429, https://doi.org/10.1016/j.indcrop.2012.12.019.
[74] R. Gupta, P. Malik, N. Das, M. Singh, Antioxidant and physicochemical study of *Psidium guajava* prepared zinc oxide nanoparticles, J. Mol. Liq. 275 (2019) 749–767, https://doi.org/10.1016/j.molliq.2018.11.085.
[75] R.K. Ameta, K.R. Shankar, M. Singh, Plant extract: an effective medium for synthesis of metal nanoparticles, Sf J. Nanochem. Nanotechnol. ISSN: 2643-8135 1 (2018), 1008.
[76] S. Mandal, Synthesis of radioactive gold nanoparticle in surfactant medium, J. Radioanal. Nucl. Chem. ISSN: 0236-5731 299 (2014) 1209–1212.
[77] J. Turkevich, P.C. Stevenson, J. Hillier, Nucleation and growth process in the synthesis of colloidal gold, Discuss. Faraday Soc. 11 (1951) 55–75, https://doi.org/10.1039/DF9511100055.
[78] G. Frens, Controlled nucleation for the regulation of the particle size in monodisperse gold suspensions, Nature 241 (1973) 20–22, https://doi.org/10.1038/physci241020a0.
[79] M. Brust, M. Walker, D. Bethell, D.J. Schiffrin, R. Whyman, Synthesis of thiol-derivatised gold nanoparticles in a two-phase liquid-liquid system, Chem. Soc. Chem. Commun. 7 (1994) 801–802, https://doi.org/10.1039/C39940000801.
[80] M.T. Reetz, W. Helbig, S.A. Quaiser, U. Stimming, N. Breuer, R. Vogel, Visualization of surfactants on nanostructured palladium clusters by a combination of STM and high-resolution TEM, Science 267 (1995) 367–369, https://doi.org/10.1126/science.267.5196.367.
[81] Y.Z. Song, X. Li, Y. Song, Z.P. Cheng, H. Zhong, J.M. Xu, J.S. Lu, C.G. Wei, A. F. Zhu, F.Y. Wu, J. Xu, Electrochemical synthesis of gold nanoparticles on the surface of multi-walled carbon nanotubes with glassy carbon electrode and their application, Russ. J. Phys. Chem. A 87 (2013) 74–79, https://doi.org/10.1134/S0036024413010275.
[82] N.R. Jana, L. Gearheart, C.J. Murphy, Seeding growth for size control of 5-40 nm diameter gold nanoparticles, Langmuir 17 (2001) 6782–6786, https://doi.org/10.1021/la0104323.
[83] R.M. Siti, A.R. Khairunisak, A.Z. Azlan, R. Noordin, Green synthesis of 10 nm gold nanoparticles via seeded-growth method and its conjugation properties on lateral flow immunoassay, Adv. Mater. Res. 686 (2013) 8–12, https://doi.org/10.4028/www.scientific.net/AMR.686.8.
[84] K.S. Kim, S. Choi, J.H. Cha, S.H. Yeon, H. Lee, Facile one-pot synthesis of gold nanoparticles using alcohol ionic liquids, J. Mater. Chem. 16 (2006) 1315–1317, https://doi.org/10.1039/b601478j.
[85] K.S. Kim, D. Demberelnyamba, H. Lee, Size-selective synthesis of gold and platinum nanoparticles using novel thiol functionalized ionic liquids, Langmuir 20 (2004) 556–560, https://doi.org/10.1021/la0355848.
[86] H. Itoh, K. Naka, Y. Chujo, Synthesis of gold nanoparticles modified with ionic liquid based on the imidazolium cation, J. Am. Chem. Soc. 126 (2004) 3026–3027, https://doi.org/10.33263/BRIAC141.012.
[87] B.R. Gangapuram, R. Bandi, M. Alle, R. Dadigala, G.M. Kotu, V. Guttena, Microwave assisted rapid green synthesis of gold nanoparticles using *Annona squamosa* L peel extract for the efficient catalytic reduction of organic pollutants, J. Mol. Struct. 1167 (2018) 305–315, https://doi.org/10.1016/j.molstruc.2018.05.004.
[88] D. Cempel, M.T. Nguyen, Y. Ishida, T. Yonezawa, L-arginine-stabilized highly uniform ag nanoparticles prepared in a microwave-induced plasma-in-liquid process (MWPLP), Bull. Chem. Soc. Jpn. 91 (2018) 362–367, https://doi.org/10.1246/bcsj.20170327.
[89] K. Jayaramulu, S. Mukherjee, D.M. Morales, D.P. Dubal, A.K. Nanjundan, A. Schneemann, J. Masa, S. Kment, W. Schuhmann, M. Otyepka, R. Zbořil, R. A. Fischer, Graphene-based metal-organic framework hybrids for applications in catalysis, environmental, and energy technologies, Chem. Rev. 122 (24) (2022) 17241–17338, https://doi.org/10.1021/acs.chemrev.2c00270.
[90] P. Malik, S.H. Mir, R. Gupta, T.K. Mukherjee, Nanographenes for renewable energy, in: Nanotechnology, Jenny Stanford Publishing, First edition, 2021, ISBN 9781003120261, https://doi.org/10.1201/9781003120261-3.
[91] I. Blakey, Z. Merican, K.J. Thurecht, A method for controlling the aggregation of gold nanoparticles: tuning of optical and spectroscopic properties, Langmuir 29 (2013) 8266–8274, https://doi.org/10.1021/la401361u.
[92] A.V. Nomoev, S.P. Bardakhanov, M. Schreibez, D.G. Bazarova, N.A. Romanaov, B. B. Baldanov, B.R. Radnaev, V.V. Syzrantsev, Structure and mechanism of the formation of core-shell nanoparticles obtained through a one-step gas-phase synthesis by electron beam evaporation, Beilstein J. Nanotechnol. 6 (2015) 874–880, https://doi.org/10.3762/bjnano.6.89.
[93] M.B. Gawande, A. Goswami, T. Asefa, H. Guo, A.V. Biradar, D.L. Peng, R. Zboril, R.S. Varma, Core-shell nanoparticles: synthesis and applications in catalysis and electrocatalysis, Chem. Soc. Rev. 44 (2015) 7540–7590, https://doi.org/10.1039/c5cs00343a.
[94] Z.Z. Dong, C. Yang, K. Vellaisamy, G. Li, C.H. Leung, D.L. Ma, Construction of a nano biosensor for cyanide anion detection and its application in environmental and biological systems, ACS Sensors 2 (2017) 1517–1522, https://doi.org/10.1021/acssensors.7b00553.
[95] X. Li, S. Li, Q. Liu, Z. Chen, Electronic-tongue colorimetric-sensor array for discrimination and quantitation of metal ions based on gold-nanoparticle aggregation, J. Anal. Chem. 91 (2019) 6315–6320, https://doi.org/10.1021/acs.analchem.9b01139.
[96] J. Li, C. Yu, Y.N. Wu, Y. Zhu, J. Xu, Y. Wang, H. Wang, M. Guo, F. Li, Novel sensing platform based on gold nanoparticle-aptamer and Fe metal-organic framework for multiple antibiotic detection and signal amplification, Environ. Int. 125 (2019) 135–141, https://doi.org/10.1016/j.envint.2019.01.033.
[97] Y. Dong, C.Y. Wen, Y. She, Y. Zhang, Y. Chen, J. Zeng, Magnetic relaxation switching immunoassay based on hydrogen peroxide-mediated assembly of ag@au-Fe_3O_4 nanoprobe for detection of aflatoxin B1, Small 17 (51) (2021) e2104596, https://doi.org/10.1002/smll.202104596.
[98] X. Yuan, H. Cao, H. Zhang, G. Mao, L. Wei, Color-encoded *Escherichia coli* assay via enzyme-induced etching of au@MnO_2 nanoparticles, Spectrochim. Acta A Mol. Biomol. Spectrosc. 299 (2023) 122888, https://doi.org/10.1016/j.saa.2023.122888.
[99] M.M. Hassan, W. Ahmad, M. Zareef, Y. Rong, Y. Xu, T. Jiao, P. He, H. Li, Q. Chen, Rapid detection of mercury in food via rhodamine 6G signal using surface-enhanced Raman scattering coupled multivariate calibration, Food Chem. 358 (2021) 129844, https://doi.org/10.1016/j.foodchem.2021.129844.
[100] E. Seker, M.L. Reed, M.R. Begley, Nanoporous gold: fabrication, characterization, and applications, Materials (Basel). 2 (2009) 2188–2215, https://doi.org/10.3390/ma2042188.
[101] D. Zhu, Q. Li, X. Pang, Y. Liu, X. Wang, G. Chen, A sensitive electrochemical impedance immunosensor for determination of malachite green and leucomalachite green in aqueous environment, Anal. Bioanal. Chem. 408 (2016) 5593–5600, https://doi.org/10.1007/s00216-016-9660-3.
[102] M.F. Wu, Y. Wang, S. Li, X.X. Dong, J.Y. Yang, Y.D. Shen, H. Wang, Y.m. Sun, H. T. Lei, Z.L. Xu, Ultrasensitive immunosensor for acrylamide based on chitosan/SnO_2-SiC hollow sphere nanochains/gold nanomaterial as signal amplification, Anal. Chim. Acta 1049 (2018) 188–195, https://doi.org/10.1016/j.aca.2018.10.041.

[103] A. Iqbal, J. Liu, B. Dixon, B. Zargar, S.A. Sattar, Development and application of DNA-aptamer-coupled magnetic beads and aptasensors for the detection of *Cryptosporidium parvum* oocysts in drinking and recreational water resources, Can. J. Microbiol. 65 (2019) 851–857, https://doi.org/10.1139/cjm-2019-0153.
[104] E. Costa-Rama, H.P.A. Nouws, C. Delerue-Matos, M.C. Blanco-Lopez, M. T. Fernandez-Abedul, Pre-concentration and sensitive determination of the anti-inflammatory drug diclofenac on a paper-based electroanalytical platform, Anal. Chim. Acta 1074 (2019) 89–97, https://doi.org/10.1016/j.aca.2019.05.016.
[105] Z. Zhang, H. Karimi-Maleh, In situ synthesis of label-free electrochemical aptasensor-based sandwich-like AuNPs/PPy/$Ti_3C_2T_x$ for ultrasensitive detection of lead ions as hazardous pollutants in environmental fluids, Chemosphere 324 (2023) 138302, https://doi.org/10.1016/j.chemosphere.2023.138302.
[106] F. Behoftadeh, M.F. Ghasemi, A. Mojtahedi, K. Issazadeh, M. Golshekan, S. Alaei, Development of a newly designed biosensor using multi-walled carbon nanotubes (MWCNTs) with gold nanoparticles (AuNPs) in the presence of acetaminophen for detection of *Escherichia coli*, Arch. Microbiol. 205 (2003) 70, https://doi.org/10.1007/s00203-023-03418-x.
[107] P. Tiet, K.C. Clark, J.O. McNamara, J.M. Berlin, Colorimetric detection of *Staphylococcus aureus* contaminated solutions without purification, Bioconjug. Chem. 28 (2017) 183–193, https://doi.org/10.1021/acs.bioconjchem.6b00571.
[108] Y. Wang, L. Wang, J. Xue, J. Dong, J. Cai, X. Hua, M. Wang, C. Zhang, F. Liu, Signal-amplified lateral flow test strip for visual detection of Cu^{2+}, PLoS One 12 (2017) e0169345 https://doi.org/10.1371/journal.pone.0169345.
[109] V. Hong, S.I. Presolski, C. Ma, M.G. Finn, Analysis and optimization of copper-catalyzed azide-alkyne cycloaddition for bioconjugation, Angrew Chem. Int. Ed. Engl. 48 (2009) 9879–9883, https://doi.org/10.1002/anie.200905087.
[110] W. Chai, Q. Feng, M. Nie, C. Wang, Y. Jiang, H. Zheng, M.J. Li, Gold nanoparticle-based probe for colorimetric detection of copper ions, J. Nanosci. Nanotechnol. 17 (2017) 502–506, https://doi.org/10.1166/jnn.2017.12419.
[111] C. Zhang, P. Du, Z. Jiang, M. Jin, G. Chen, X. Cao, X. Cui, Y. Zhang, R. Li, A.M. A. El-Aty, J. Wang, A simple and sensitive competitive bio-barcode immunoassay for triazophos based on multi-modified gold nanoparticles and fluorescent signal amplification, Anal. Chim. Acta 999 (2018) 123–131, https://doi.org/10.1016/j.aca.2017.10.032.
[112] P. Xie, L. Zhu, X. Shao, K. Huang, J. Tian, W. Xu, Highly sensitive detection of lipopolysaccharides using an aptasensor based on hybridization chain reaction, Sci. Rep. 6 (2016) 29524, https://doi.org/10.1038/srep29524.
[113] J. Zhang, I. Khan, Q. Zhang, X. Liu, J. Dostalek, B. Liedberg, Y. Wang, Lipopolysaccharides detection on a grating-coupled surface plasmon resonance smartphone biosensor, Biosens. Bioelectron. 99 (2018) 312–317, https://doi.org/10.1016/j.bios.2017.07.048.
[114] S. Gupta, S. Huda, P.K. Kilpatrick, O.D. Velev, Characterization and optimization of gold nanoparticle-based silver-enhanced immunoassays, Anal. Chem. 79 (2007) 3810–3820, https://doi.org/10.1021/ac062341m.
[115] H. Manoharan, P. Kalita, S. Gupta, V.V.R. Sai, Plasmonic biosensors for bacterial endotoxin detection on biomimetic C-18 supported fiber optic probes, Biosens. Bioelectron. 129 (2019) 79–86, https://doi.org/10.1016/j.bios.2018.12.045.
[116] M. Elumalai, A. Ipatov, J. Carvalho, J. Guerreiro, M., Prado dual colorimetric strategy for specific DNA detection by nicking endonuclease-assisted gold nanoparticle signal amplification, Anal. Bioanal. Chem. 14 (2022) 5239–5253, https://doi.org/10.1007/s00216-021-03564-5.
[117] X. Wang, R. Nag, N.P. Brunton, M.A.B. Siddique, S.M. Harrison, F.J. Monahan, E. Cummins, Human health risk assessment of bisphenol a (BPA) through meat products, Environ. Res. 213 (2022) 113734, https://doi.org/10.1016/j.envres.2022.113734.
[118] J. Liu, L. Zhang, G. Lu, R. Jiang, Z. Yan, Y. Li, Occurrence, toxicity and ecological risk of bisphenol a analogues in aquatic environment- a review, Ecotoxicol. Environ. Saf. 208 (2021) 111481, https://doi.org/10.1016/j.ecoenv.2020.111481.
[119] S. Ren, S. Cho, R. Lin, V. Gedi, C.W. Sunyoung Park, D.K. Ahn, M.H. Lee, S. Lee, S. Kim Lee, Nonbiodegradable Spiegelmer-driven colorimetric biosensor for Bisphenol A detection, Biosensors 12 (2022) 864, https://doi.org/10.3390/bios12100864.
[120] W. Ye, M. Yu, F. Wang, Y. Li, C. Wang, Multiplexed detection of heavy metal ions by single plasmonic nanosensors, Biosens. Bioelectron. 196 (2022) 113688, https://doi.org/10.1016/j.bios.2021.113688.
[121] S. Syama, P.V. Mohanan, Comprehensive application of graphene: emphasis on biomedical concerns, Nano-Micro Lett. 11 (2019), https://doi.org/10.1007/s40820-019-0237-5.
[122] S. Priyadarsini, S. Mohanty, S. Mukherjee, S. Basu, M. Mishra, Graphene and graphene oxide as nanomaterials for medicine and biology application, J. Nanostructure Chem. 8 (2018) 123–137, https://doi.org/10.1007/s40097-018-0265-6.
[123] W.L. Daniel, M.S. Han, J.S. Lee, C.A. Mirkin, Colorimetric nitrite and nitrate detection with gold nanoparticle probes and kinetic end points, J. Am. Chem. Soc. 131 (2009) 6362–6363, https://doi.org/10.1021/ja901609k.
[124] P.U. Maheswari, B. Modec, A. Pevec, B. Kozlevca, C. Massera, P. Gamez, J. Reedijk, Crystallographic evidence of nitrate-pi interactions involving the electron-deficient 1,3,5-triazine ring, Inorg. Chem. 45 (2006) 6637–6645, https://doi.org/10.1021/ic060101j.
[125] Y. Li, P. Wu, H. Xu, Z. Zhang, X. Zhong, Highly selective and sensitive visualizable detection of hg^{+2} based on anti-aggregation of gold nanoparticles, Talanta 84 (2011) 508–512, https://doi.org/10.1016/j.talanta.2011.01.037.
[126] W. Ren, S. Mura, J.M.K. Irudayaraj, Modified graphene oxide sensors for ultra-sensitive detection of nitrate ions in water, Talanta 143 (2015) 234–239, https://doi.org/10.1016/j.talanta.2015.05.073.
[127] A. Maity, X. Sui, C.R. Tarman, H. Pu, J. Chang, G. Zhou, R. Ren, S. Mao, J. Chen, Pulse-driven capacitive lead ion detection with reduced graphene oxide field-effect transistor integrated with an analyzing device for rapid water quality monitoring, ACS Sens. 2 (2017) 1653–1661, https://doi.org/10.1021/acssensors.7b00496.
[128] J. Guan, K. He, S. Gunasekaran, Self-assembled tetrahedral DNA nanostructures-based ultrasensitive detection of ampicillin, Talanta 243 (2022) 123292, https://doi.org/10.1016/j.talanta.2022.123292.
[129] H. Moulahoum, Dual chromatic laser-printed microfluidic paper-based analytical device (μPAD) for the detection of atrazine in water, ACS Omega 8 (2023) 41194–41203, https://doi.org/10.1021/acsomega.3c04387.